AD-A113 020 MASSACHUSETTS INST OF TECH CAMBRIDGE FLUID MECHANICS LAB F/G 20/4
MEASUREMENT METHODS FOR FLUID SHEAR STRESS.(U)
MAR 82 C F DEWEY, P W HUBER N00014-80-C-0109
UNCLASSIFIED 82-4 NL

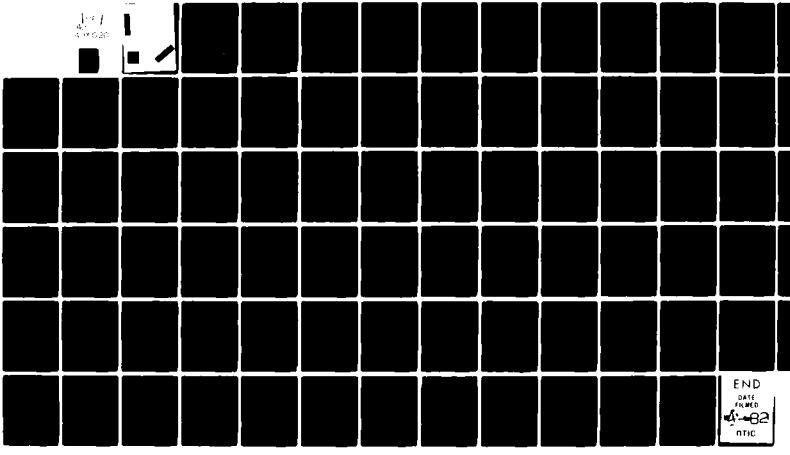

END
DATE FILMED
4-82
DTIC

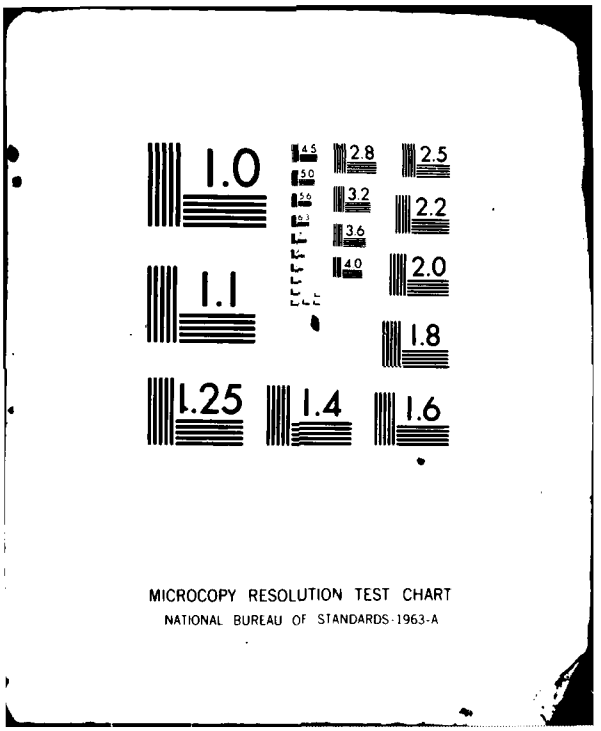
1.0
1.1
1.25
1.4
1.6
1.8
2.0
2.2
2.5
2.8
3.2
3.6
4.0
4.5
5.0
5.6
MICROCOPY RESOLUTION TEST CHART
NATIONAL BUREAU OF STANDARDS-1963-A

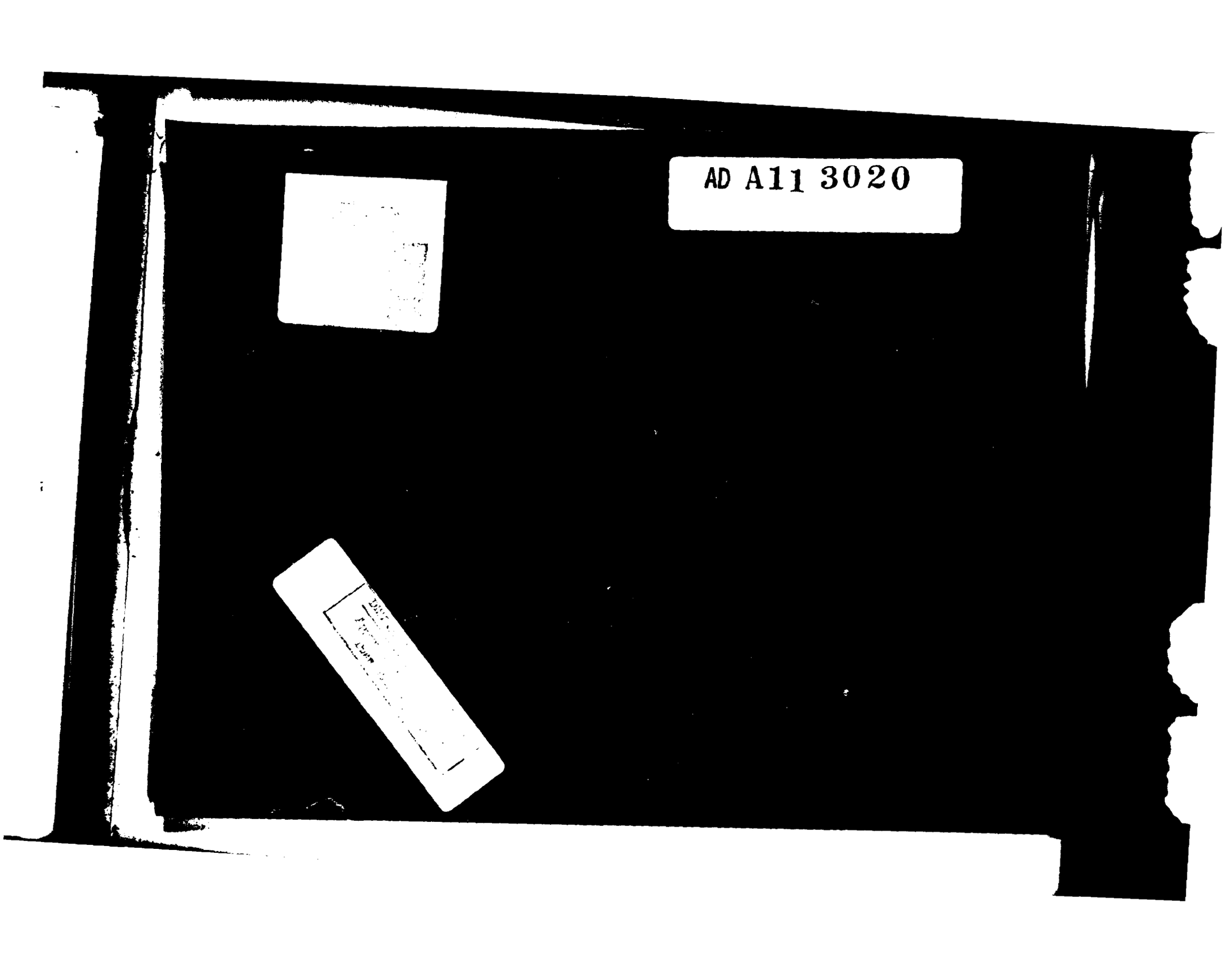

(1)

Annual Summary Report
Covering the Period 1 January to 31 December, 1980

MEASUREMENT METHODS FOR FLUID SHEAR STRESS

by

C. Forbes Dewey, Jr. and Peter W. Huber

March 1982

Fluid Mechanics Laboratory
Department of Mechanical Engineering
Massachusetts Institute of Technology
Cambridge, Massachusetts 02139

Research Sponsored by

Office of Naval Research
M.K. Ellingsworth, Program Monitor
Arlington, Virginia 22217

ONR Contract N 00014-80-C-0109
ONR Contract Authority NR-097-441

MEASUREMENT METHODS FOR FLUID SHEAR STRESS

C. Forbes Dewey, Jr. and Peter W. Huber
Fluid Mechanics Laboratory
Massachusetts Institute of Technology
Cambridge, MA 02139

ABSTRACT

Fluid shear stress is one of the most important quantities characterizing the interaction between a flowing fluid and a solid body. A knowledge of surface shear stress is essential in determining the drag on submerged bodies, the energy losses in internal flows, local surface heat transfer rates in both internal and external flows, flow separation, cavitation, and unsteady flow behavior in rotating machinery.

In spite of many previous investigations of both laser Doppler anemometry (LDA) and surface hot-film gauges, the use of these methods for determining wall shear stress is poorly developed. Conventional LDA measurements near surfaces are plagued by spurious background scattering and marginal resolution. Use of surface hot-film gauges is severely inhibited by the necessity of empirical calibration and an incomplete understanding of their response in turbulent and unsteady flows.

This research program is developing new methodology for the use of these two complementary techniques as quantitative measurement tools for determining local surface shear stress. The LDA system is based on detecting laser-induced fluorescence from solid particles in a so-called "backscatter" mode. Two individual velocity components can be measured by using multiplexing in frequency domain. The hot-film probes employ multiple elements such that conventional calibration procedures can be eliminated. Both theory and experiment are used to determine the utility of LDA and hot-film instrumentation in unsteady flows.

REPORT DOCUMENTATION PAGE		READ INSTRUCTIONS BEFORE COMPLETING FORM
1. REPORT NUMBER N 0014-80C-0109-002	2. GOVT ACCESSION NO. AD-A113 620	3. RECIPIENT'S CATALOG NUMBER
4. TITLE (and Subtitle) MEASUREMENT METHODS FOR FLUID SHEAR STRESS		5. TYPE OF REPORT & PERIOD COVERED Jan. 1,1980 to Dec. 31,1980 6. PERFORMING ORG. REPORT NUMBER
7. AUTHOR(s) C. Forbes Dewey, Jr. and Peter W. Huber		8. CONTRACT OR GRANT NUMBER(s) N00014-80-C-0109
9. PERFORMING ORGANIZATION NAME AND ADDRESS Dept. of Mechanical Engineering Massachusetts Institute of Technology Cambridge, MA 02139		10. PROGRAM ELEMENT, PROJECT, TASK AREA & WORK UNIT NUMBERS Contract Authority NR097-441
11. CONTROLLING OFFICE NAME AND ADDRESS Office of Naval Research 800 North Quincy Street Arlington, Virginia 22217		12. REPORT DATE March 1982 13. NUMBER OF PAGES 78
14. MONITORING AGENCY NAME & ADDRESS(if different from Controlling Office)		15. SECURITY CLASS. (of this report) Unclassified 15a. DECLASSIFICATION/DOWNGRADING SCHEDULE

16. DISTRIBUTION STATEMENT (of this Report)

Approved for public release; distribution unlimited

17. DISTRIBUTION STATEMENT (of the abstract entered in Block 20, if different from Report)

18. SUPPLEMENTARY NOTES

19. KEY WORDS (Continue on reverse side if necessary and identify by block number)

Fluid Flow, Heat Transfer, Fluid Shear Stress, Laser Doppler Anemometry, Hot-Film Gauges.

20. ABSTRACT (Continue on reverse side if necessary and identify by block number)

Fluid shear stress is one of the most important quantities characterizing the interaction between a flowing fluid and a solid body. A knowledge of surface shear stress is essential in determining the drag on submerged bodies, the energy losses in internal flows, local surface heat transfer rates in both internal and external flows, flow separation, cavitation, and unsteady flow behavior in rotating machinery.

In spite of many previous investigations of both laser Doppler anemo-

metry (LDA) and surface hot-film gauges, the use of these methods for determining wall shear stress is poorly developed. Conventional LDA measurements near surfaces are plagued by spurious background scattering and marginal resolution. Use of surface hot-film gauges is severely inhibited by the necessity of empirical calibration and an incomplete understanding of their response in turbulent and unsteady flows.

This research program is developing new methodology for the use of these two complementary techniques as quantitative measurement tools for determining local surface shear stress. The LDA system is based on detecting laser-induced fluorescence from solid particles in a so-called "backscatter" mode. Two individual velocity components can be measured by using multiplexing in the frequency domain. The hot-film probes employ multiple elements such that conventional calibration procedures can be eliminated. Both theory and experiment are used to determine the utility of LDA and hot-film instrumentation in unsteady flows.

TABLE OF CONTENTS

I. DESCRIPTION OF PROGRAM

A. Rationale

The vast majority of all energy conversion processes involve fluid flow and heat transfer. The performance of gas turbines, compressors, heat exchangers, and other equipment used to generate power cannot be optimized without extensive theoretical and experimental research. And a key element in this research is the ability to make accurate measurements of detailed flow characteristics within the devices being tested.

The importance to the ONR Power Program of fluid flow and hear transfer research, including research on measurement techniques, may be judged by the numerous research projects being supported in these areas. A series of workshops have been sponsored by Project SQUID to assess progress in particular aspects of fluid flow research; since 1969, three conferences have explored gas dynamics and unsteady flow phenomena, two have been devoted to turbulence, and three have had the theme of laser instrumentation for fluid flow measurement. As one reads the Proceedings of these workshops [e.g. Murthy (1976)], it becomes clear that complicated three-dimensional unsteady flows are of utmost importance; and our ability to make accurate measurements in such environments is severely limited.

Fluid shear stress is one of the most important experimental quantitites characterizing the interaction between a flowing fluid and a solid body. A knowledge of surface shear stress is essential in determining the drag on submerged bodies, the energy losses in internal flows, local surface heat transfer rates in both external and internal flows, flow separation, cavitation, and unsteady flow behavior in rotating devices. High-frequency fluctuations of shear stress can pinpoint acoustic modes in inlets and ducts, or detect unsteady shock-induced boundary layer separation. Local shear stress (both magnitude and direction) is a quantity that, in some cases, may be predicted by theory; and comparison between theory and experiment for this quantity is a sensitive test of the accuracy of the calculation procedure.

There are only two practical methods of measuring the fluid shear stress acting on a variety of solid surfaces: laser Doppler anemometry (LDA) to determine the fluid velocity profile near the wall, thereby obtaining the shear rate and, with knowledge of the fluid viscosity, the shear stress; and the surface hot-film gauge whose rate of heat loss can be related to local shear stress by appropriate calibration. Other methods (e.g. Preston Tube, hot-wire anemometers, electrochemical probes, and floating-element balances) have inherent limitations that preempt their use in most practical circumstances.

B. Objectives

The objectives of our research program are as follows:

(1) Develop a comprehensive first-principles description of the thermal response of surface hot-film gauges to imposed fluid flow. The theory will include complete 3-dimensional transient conduction to the substrate and a time-dependent quadratic fluid velocity profile. Experimental verification will be obtained for quartz-backed and poly (vinylidine fluoride) lithographed gauges in our pulsatile flow facility and cone-plate calibration apparatus.

(2) Develop a two-component backscatter LDA system with fluorescent seed particles for optimum S/N ratio and improved spatial resolution near solid surfaces. Bragg-shift multiplexing of a single excitation wavelength will be used to provide two orthogonal velocity components. Make a direct comparison between 2-component LDA using fluorescence and conventional 2-component system using two different wavelengths.

(3) Produce a detailed quantitative comparison between LDA and hot-film instruments in standard laminar and turbulent flow regimes (pulsatile flow, pipe flow, cone-plate laminar and turbulent flow). Refine interpretation of the hot-film response on the basis of measured turbulent sub-layer velocity components including intermittent sweeps.

The shear stress measurement techniques that we are developing will have substantial potential value to a wide variety of problems of interest to the Navy. Measurements within complex heat exchanger geometries will

provide valuable data for understanding local heat transfer coefficients.

Measurements can be made on turbine and compressor models to detect flow separation and to unravel complex flow velocity patterns that defy theoretical or conventional experimental methods. Measurements may also be easily made on large ship models and full-scale vessels of local friction drag.

(4) Fabricate multiple-film gauges using microlithography and thick-film technology to achieve a self-calibrated sensor with sufficient information to give shear direction as well as magnitude.

(5) Apply these composite hot-film gauges to high-speed unsteady flow.

(6) Develop quantitative assessments and recommendations regarding relative ease of use, accuracy, and cost of LDA vs. hot-film technology for measuring wall shear stress in a variety of flows of interest.

C. Personnel

The following personnel participated in the program during the current contract period:

C. Forbes Dewey, Jr.	-	Co-Principal Investigator
Peter W. Huber	-	Co-Principal Investigator
Kenneth M. Kalumuck	-	Research Assistant
Don F. Pardo	-	Research Assistant
Leanna Tyau	-	Research Assistant
Judi Steciak	-	Research Assistant
Richard Struve	-	Research Assistant
Marj Joss	-	Secretary
R. Fenner	-	Research Staff Member

D. Major Accomplishments for Current Reporting Period

Fig. 1 is a table summarizing important previous theoretical calculations of hot-film probe heat transfer to a flowing fluid. The current theory being developed by Ken Kalumuck is substantially more complete in representing the conditions existing in practice than any previous efforts in this area. The

work of Pardo, completed with partial support from the current program, in our laboratory, was important in establishing the quantitative importance of substrate conduction.

Kalumuck considers a thin film on a wall surface (the x-z plane) exposed to a flowing fluid. The film is of arbitrary shape and an amount of heat q(x,z) per unit area is generated by the film. Some heat is conducted into the wall, and additional heat is given up directly to the fluid.

A solution to the coupled heat conduction and fluid convection equations is obtained. First, the equations are subjected to Fourier transformation in two of the three spatial directions. This leads to two ordinary differential equations in y (the coordinate normal to the wall). The solution to these equations is then obtained in terms of the transformed variables. As a final step, a two-dimensional Fast Fourier Transform (FFT) is performed to obtain the detailed temperature field in any desired x-z plane. The resulting solution includes all of the detailed information on heat flux both to the solid and to the fluid. Specific results have been obtained and are reported in Section II.

Preliminary results have been obtained by R. Struve using an ion laser to excite fluorescent particles and using the fluorescence to track the particles. From these experimental results and the calculations of L. Tyau, we expect that our technique of using fluorescent particles in the LDA experiments will be successful. The details of these results will be found in Section III.

STEADY FLOW HOT-FILM MODELS

Model	Geometry	Streamwise conduction	Substrate conductivity	Probe condition*
Leveque	2-d	-	-	U T
Ling	2-d	x	-	U T
Tanner	pseudo 3-d	-	x	U Q; retangular
Davies & Kimber	2-d	x	x	U Q
Ackerberg, et. al.	2-d	x	-	U T; small Peclet number
Pardo	2-d	x	x	U T
Current work	3-d	x	x	arbitrary shape and flux distribution

*
U T : uniform temperature
U Q : uniform heat flux

FIG. 1

II. HOT-FILM GAUGES FOR MEASURING FLUID SHEAR STRESS

A. Review of Literature

Hot-film elements [Ludweig (1950)] have been used for many years to measure flow velocities and wall shear in a variety of fluid flow applications. Methodology important to their use was first developed by Liepmann and Skinner (1955) and Ling (1955). Important contributions to the theoretical interpretation of the relation between heat and momentum transfer for such probes was made by Lighthill (1954), and Ling (1963), and subsequently by Brown (1967), Spence and Brown (1968), Ackerberg et al. (1978), Springer and Pedley (1973), and (using a mass transfer analogy) Hanratty and colleagues [Fortuna and Hanratty (1962, 1963), and Sirkar and Hanratty (1970a, 1970b)]. A current review by Hanratty and Campbell is also in press [Hanratty (1982)].

Among the more important examples of the use of hot-film techniques are those of Ling et al. (1968, 1969), Bellhouse and Schultz (1967, 1968), Brech and Bellhouse (1973), Clark (1974), Armistead and Keyes (1968), Eckelmann and Reichardt (1971), Pope (1971), Geremia (1970), McCroskey and Durbin (1972), and Murthy and Rose (1978).

The principle of operation of a hot-film gauge is simple: the rate of removal of heat from a small heated film is related to the instantaneous shear stress (or more precisely, the velocity gradient) in the fluid immediately adjacent to the film. Important experimental difficulties and theoretical limitations to the accurate quantitative use of such gauges have been identified previously and are discussed in the following sections. But the potential advantages of hot-film gauges over existing alternatives are clear. Hot-film gauges are physically small and require no more wiring or peripheral instrumentation close to the measuring point than does a pressure transducer or conventional strain gauge. They can operate in opaque liquids or at optically inaccessible points within rotating machinery, piping systems and valves. They can be designed to withstand corrosive or otherwise hostile environments. Flush mounting on a wall can assure that the measurement process will result in minimal disturbance to the fluid phenomena under

investigation. The gauges are *potentially* inexpensive and simple to use; that they cannot be described in this way at present can be attributed primarily to: (1) difficulties encountered in accurate calibrations; and (2) substantial uncertainty with regard to the interpretation of the hot-film signal in unsteady and turbulent flows. The promise of this instrument is nonetheless clear; the hot-film gauge could become as versatile and easy to use in measuring rates of strain (or shear stresses) in fluids as are conventional strain gauges for measuring ordinary strains in solids.

The underlying principle of operation of thin film shear stress gauges stems from the Reynolds analogy between heat transfer and local skin friction coefficient in laminar two-dimensional boundary layers in which heating effects due to friction and fluid compression are negligible. In its general form the Reynolds analogy emerges directly from the boundary layer momentum and energy equations [Schlichting (1968)] and states that the heat transfer to or from a wall is related to the shear stress at the wall by a function of the form:

$$Nu = 0.5\, c_f \cdot Re \cdot \Phi\left(\frac{x}{\ell}, Pr\right) \tag{1}$$

where Φ represents a functional dependence that includes the upstream history of the boundary layer. Here the Nusselt, Reynolds and Prandtl numbers and the skin friction coefficient are defined in the usual way:

$$Nu = \frac{q\ell}{K(T_w - T_\infty)} \tag{2}$$

$$Re \equiv \frac{U_\infty \ell}{\nu} \tag{3}$$

$$Pr \equiv \frac{\nu}{\alpha} \tag{4}$$

$$c_f = \frac{\mu\left(\frac{\partial u}{\partial y}\right)_w}{\frac{1}{2}\rho_\infty U_\infty^2} \tag{5}$$

In Eqs. (1) -(5), x and y are coordinates of position parallel to and perpendicular to the wall, q is the local heat transfer rate per unit area, ℓ is a characteristic length scale in the flow direction, k is the fluid thermal conductivity, T_w is the local wall temperature, U_∞, ρ_∞, and T_∞ are the free stream fluid velocity, density and temperature, and ν and α the fluid kinematic viscosity and thermal diffusivity ($k/\rho c_p$) respectively; $(\partial u/\partial y)_w$ denotes the local velocity gradient at the wall.

The theory for the operation of thin film gauges follows directly from Eq. (1). If we consider the case of a thin heated film of length L and width W mounted flush with an adiabatic wall, with the film temperature T_w (Figure 1), then for any given laminar flow velocity profile

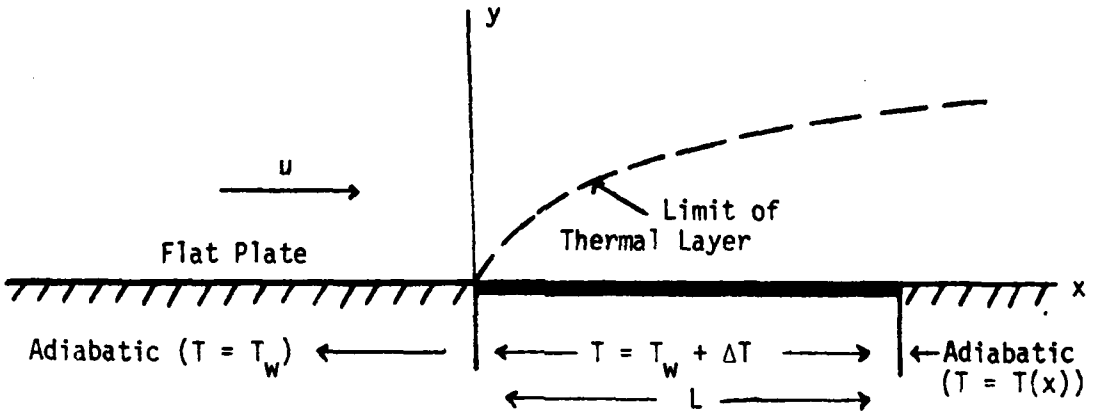

Figure 1. Laminar flow over a heated strip.

above the film it is possible to correlate the rate of heat transfer from the film to the fluid with the shear stress at the wall. For the case of a velocity profile that can be considered linear over a distance

from the wall larger than the thermal boundary layer thickness above the probe, the functional relation in Eq. (1) can be determined exactly [Lévéque (1928)]. Averaging the heat transfer over the film surface for this case one obtains

$$\overline{Nu} = \frac{\bar{q}\,L}{K(T_w - T_\infty)} = 0.807\, N_L^{1/3} \tag{6}$$

$$N_L \equiv Pr\,\frac{L^2}{\nu}\left(\frac{\partial u}{\partial y}\right)_w \equiv Pr\left(\frac{Lu_*}{\nu}\right)^2 \tag{7}$$

$$u_*^2 \equiv \nu\left(\frac{\partial u}{\partial y}\right)_w \tag{8}$$

The average heat transfer rate per unit area, $\bar{q}$, may be equated to the electrical dissipation in the probe divided by the size of the probe, i.e.

$$q = \left(\frac{V^2}{R}\right)\frac{1}{W \cdot L} \tag{9}$$

where V is the voltage across the thin film, R is the film resistance, and L and W are, respectively, the film dimensions in the direction of flow and normal to it. It is frequently assumed that the two-dimensional analysis leading to Eq. (6) is valid if $L \ll W$; this is not, in fact, the case.

In practice, Eq. (6) does not hold because the wall is *not* adiabatic and heat conduction occurs into the solid.* This leads to heating of the fluid in the boundary layer upstream of the probe and, in general, a transfer of heat from the heated fluid into the wall downstream of the probe.

*For moderately-conducting solids, the thermal penetration depth into the solid is comparable to the probe length W, and the heat conduction problem is 3-dimensional.

Eq. 6 suggests that the relation between the measured electrical heat dissipation and shear stress is of the form

$$Nu_M = A + B \left(\frac{\partial u}{\partial y}\right)_w^{1/3} \tag{10}$$

where A and B are constants to be found by calibration, Nu_M is the measured Nusselt number obtained by substituting Eq. (9) into Eq. (2), and ΔT is assumed to be fixed for both the calibration and the conditions of use.

Before proceeding, it should be recognized that the flow-independent term, "A", in Eq. (10) is often 2 to 4 times *larger* than the term containing information on the local shear stress. This term arises primarily from substrate conduction [Tanner (1967)] and is relatively insensitive to natural convection [Ackerberg et al. (1978)]. Measurement sensitivity is increased by decreasing substrate conduction (reducing "A" relative to "B $(\partial u/\partial y)_w$"); but this imposes certain difficulties with regard to the interpretation of measurements in unsteady flows.

Our experience [c.f. Sdougos (1977)] as well as the experience of most other investigators [c.f. Pope (1971), Bellhouse and Schultz (1966), Geremia (1970), Brown and Davey (1971), and Murthy and Rose (1978)] is that Eq. (10) represents an excellent fit to laminar steady-flow calibration experiments under conditions where the parameter N_L is moderately large, say $N_L \gtrsim 20$. For smaller values of N_L, the theory of Ackerberg *et al.* (1978) may be consulted. In flows with pressure gradients, for which the region of linear velocity variation is reduced (Fig. 2), additional terms in Eq. (10) are necessary [see Spence and Brown (1968)].

The fact remains, however, that conventional use of hot-film shear stress gauges, *even in steady laminar flow*, requires calibration under conditions closely approximating those of the proposed measurements. This is an extremely tedious and cumbersome procedure. One principal objective of our research is to substantially reduce (effectively eliminate) the tedious calibration procedures that are presently required.

There is very little quantitative information available in the literature on the response of hot-film gauges to unsteady shear. Although the electrical response time of the film and feedback circuit is many KHz, the gauge cannot respond in a quasi-steady manner to the

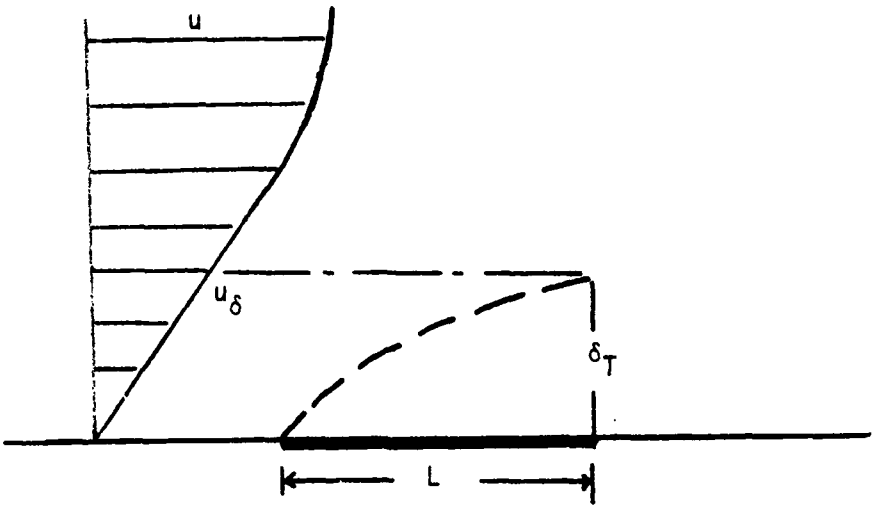

Figure 2. The thermal boundary layer growing into a linear shear flow.

imposed shear stress fluctuations unless the convective heat transfer *and* the substrate conduction heat transfer approach a steady state within a time comparable to that between fluctuations.

To understand the nature of this problem, we consider the response of a heated film to flow fluctuations imposed upon it by the external flow. The easiest case to consider is a flat plate, upon which a thin film gauge is mounted, that oscillates parallel to its surface. In a coordinate system moving with the surface, this is equivalent to an oscillating boundary layer immediately above the plate -- a problem treated by Lighthill (1954), Bellhouse and Schultz (1968), and Fortuna and Hanratty (1971). Experimental evidence is available from Fortuna (1970), Ling et al. (1968) and, for free probes, Clark (1974). We wish to present a simple physical argument for

estimating the upper frequency limit for which the steady-state relation of Eq. (1) between wall shear stress and measured heat transfer is valid. It will then be shown that this simple model reproduces the essential features of the more rigorous solution of Fortuna and Hanratty (1971).

Referring to Fig. 2, we define u_δ to be the fluid velocity at a height δ_T above the surface. It is clear that the thermal boundary layer developing along the strip will not be quasi-steady unless the fluid particles heated by the strip have nearly constant velocity during their passage past the strip. This suggests that a particle moving along a streamline δ_T above the plate should travel a distance of at least 10L during one cycle of the imposed velocity fluctuation of frequency ω_L in order to insure quasi-steady behavior; i.e.

$$\omega_F \equiv 2\pi f < 2\pi \left(\frac{u_\delta}{10L} \right) . \tag{11}$$

The magnitude of u_δ for a probe operating in the linear velocity regime (Fig. 2) is equal to the velocity gradient, $(\partial u/\partial y)_w$, times the height, δ_T, of the thermal layer at the rear of the strip. From Ling (1963),

$$\frac{\delta_T}{L} \cong \frac{2.9}{N_L^{1/3}} \tag{12}$$

where

$$N_L = Pr \frac{L^2(\partial u/\partial y)_w}{\nu} \equiv Pr \left(\frac{Lu_*}{\nu} \right)^2$$

$$\equiv Pr\, L^{*2} \tag{13}$$

$$L^* \equiv Lu_*/\nu$$

$$u_* \equiv \left[\nu(\partial u/\partial y)_w \right]^{1/2} \tag{14}$$

Inserting Eqs. (12) and (13) into (11), we have the restriction on frequency for quasi-steady probe response:

$$\omega_F < 1.8 \frac{(\partial u/\partial y)_w}{[Pr\, L^{*2}]^{1/3}} \tag{15}$$

This result may be cast into a form suitable for comparison with the results of Fortuna and Hanratty (1971). We define a nondimensional frequency

$$\omega_F^* \equiv \frac{\omega_F \nu}{u_*^2} Pr^{1/3} \tag{16}$$

By using Eqs. (13) -(14), we have the simple form for the present model:

$$\omega_F^* L^{*2/3} < 1.8 \tag{17}$$

Fortuna and Hanratty have calculated the ratio, A^2, of the mean square fluctuation amplitude of the heat transfer to a flow disturbance of frequency ω to the amplitude of the induced heat transfer which would be measured if the flow disturbance had the same amplitude but the oscillation was very slow. Their result is:

$$A^2 = \left| 1 + 0.060\left(\omega_F^* L^{*2/3}\right)^2 \right|^{-1} \tag{18}$$

$$\left(\omega_F^* L^{*2/3} < 5^{1/2}\right)$$

For the criteria we presented in Eq. (17), $\omega_F^* L^{*2/3} < 1.8$, their calculations predict about a 20% decrease in the mean square fluctuation, or a 10% decrease in the (linear) amplitude of the heat transfer fluctuation. Referring to Eq. (6), the implied wall shear stress fluctuation would then be too low by 30%.

Some typical numbers are informative here. For a pipe flow at a characteristic velocity $V = 0.1\ ms^{-1}$ in a pipe of 0.01 m diameter with water as the liquid we have:

$$Pr = 8$$

$$\nu = 1 \times 10^{-6}\ m^2\ s^{-1}$$

$$Re = 10^3$$

$$u_* \approx 0.009\ ms^{-1}$$

$$\left(\frac{\partial u}{\partial y}\right)_w \approx 80\ s^{-1}$$

For a probe of length $L = 1.5 \times 10^{-4}$ m, $L^* = 1.35$ and from Eq. (14) the upper limit for the frequency response is found to be: $f \equiv (\omega/2\pi) < 10$ Hz. This typical calculation points out the substantial limitation to quasi-steady frequency response that hot film gauges possess.

The quasi-steady response criteria presented in Eq. (15) was obtained by considering the heat transfer from the film to the flow. Inasmuch as a substantial portion of the heat generated in the film is conducted into the substrate, quasi-steady behavior also requires that a time-independent substrate temperature distribution has been achieved. The time scale for this equilibration can be estimated from well-known solutions to unsteady heat conduction problems in solids [c.f. Carslaw and Jaeger (1947)]. The characteristic penetration depth, x_{char}, of an oscillating thermal wave into a solid is given by

$$x_{char} \approx (\kappa_s t)^{1/2}$$

where $\kappa_s \equiv (k/\rho c)$ is the thermal diffusivity of the solid. If we associate x_{char} with the probe length L and the time t with a half-period of the thermal oscillation [$\omega_s = (\pi/t)$] in the substrate, then the substrate temperature distribution will be in equilibrium provided

$$\omega_s < (\pi \kappa_s / L^2) \tag{19}$$

The ratio of limiting frequencies calculated from fluid response and substrate response is then

$$\frac{\omega_s}{\omega_F} \approx 1.7\ Pr^{1/3} \left(\frac{\kappa_s}{\nu}\right) L^{*-4/3} \tag{20}$$

One of the objectives of our program is to obtain accurate relations for the frequency response of hot-film probes. Although the arguments presented in the preceding paragraphs establish limits for the quasi-steady frequency response of the gauges to imposed shear stress fluctuations, it is not necessary to limit their use to such low frequencies *provided that the gauge transfer function is known as a function of frequency.* As Eq. (19) demonstrates, this transfer function must include the effects of substrate conduction.

Previous attempts to establish such transfer functions by empirical measurements [Armistead and Keyes (1968a, 1968b), Bellhouse and Schultz (1966), Seed and Wood (1970), Woodruffe (1970), Clark (1974)] have been inconclusive at best. In particular, Clark (1974), Smith *et al.* (1974) and Bellhouse and Schultz (1966, 1967) observed a transfer function that exceeds unity at intermediate frequencies, and rolls off approximately as ω^{-1} at high frequencies. This result is in contradiction to the monotonically decreasing transfer function predicted by Fortuna and Hanratty (1971).

Clark (1974) has remarked that the theory of Pedley (1972) [see also Pedley (1976)] might be applicable, but this theory does not predict the correct phase relationship between heat transfer and shear stress and is therefore suspect.

We anticipate that our research will encourage use of hot-film gauges in unsteady flows where a mean bulk or core flow has a periodic or fluctuating component characterized by a single frequency. If a boundary layer of thickness δ_m due to the mean flow separates the wall from the core flow region, periodic fluctuations in the core flow will be felt as shear stress fluctuations at the wall only if they are below some maximum frequency. This result is the classical problem of the "depth of penetration" of a viscous wave [Stuart (1955)]: the viscous boundary layer is impervious to shear stress fluctuations at frequencies higher than or of order:

$$\omega \gtrsim \frac{\nu}{\delta_m^2} \tag{21}$$

For a boundary layer thickness 10^{-4} m and a kinematic viscosity of 10^{-6} $m^2\ s^{-1}$ the frequency cut-off is of order 100 Hz. More will be said about the implications of this result in the paragraphs that follow.

The simplest, and at this stage probably the only, possible argument for assessing the performance of hot-film gauges in turbulent flows is that when the thermal boundary layer thickness is less than that of the laminar sublayer the principles and equations outlined and developed in the previous section should be applicable. The well-known linear velocity predictions for a sublayer extending a distance of order 5 ν/u^* above the wall are usually cited, and the requirement that the thermal boundary layer be thinner than this is thus of the form [Ling (1963); Liepmann and Skinner (1954)]:

$$\delta_T < 5\left(\frac{\nu}{\left(\frac{\partial u}{\partial y}\right)_w}\right)^{1/2} \tag{22}$$

In terms of the non-dimensional variables usually used to describe the turbulent boundary layer,

$$u^+ = (u/u_*) \tag{23}$$

$$y^+ = (yu_*/\nu) \tag{24}$$

$$u_* \equiv \left[\nu(\partial u/\partial y)_w\right]^{1/2} \tag{8}$$

this criteria becomes

$$\delta_T^+ < 5 \tag{25}$$

Estimating δ_T using Eq. (12), we have a criterion for the maximum length, L, of a hot-film gauge that would be suitable for measurements of shear stress in turbulent flow:

$$L^* \equiv (Lu_*/\nu) < 5.1\ Pr \tag{26}$$

This criterion is normally satisfied with the small values of L (10^{-4} m or less) normally employed in hot-film gauges. Such arguments, as far as they go, cannot be faulted; but there is, as yet, no proof that the Reynolds analogy holds in the laminar sublayers of turbulent flow when Eq. (26) is satisfied. It seems safe to expect that under some conditions turbulent flow wall shear stresses inferred from hot film data based on the conventional laminar boundary layer equations will be reasonably accurate. On the other hand, enough is already known about the three dimensional structures and periodic "sweeping" of laminar sublayers to suggest that parallels between ordinary laminar boundary layers and laminar sublayers are not perfect. An objective of our research program is to define the relationship between mean and fluctuating shear stresses, as measured with a hot-film gauge, and the true dynamic processes occurring in the sublayer of a turbulent boundary.

The important measurements that have been made with hot-film gauges in turbulent flow will now be reviewed.

Bellhouse and Schultz (1968) describe the measurement of laminar oscillatory shear flows superposed on large mean flows in air with a flush-mounted hot-film gauge (constant temperature mode). The authors suggested that the probe, when operating in the laminar sublayer of a turbulent flow, would respond as it would in a truly laminar rectilinearly oscillatory flow, but they did not offer any evidence to support this claim.

Armistead and Keyes (1968a, 1968b) compare the frequency spectra of heat transfer from a flush-mounted hot-film in a turbulent flow to the spectra of wall mass transfer and wall pressure fluctuations. The authors expect that fluctuations in the rates of heat and mass transfer and wall pressure fluctuations "should be closely related" since all are induced by "flow perturbations in the wall layer." This is not correct; Townsend (1976) remarks that wall pressure fluctuations are influenced by velocity fluctuations within a distance (larger than the sublayer thickness) comparable to the wavelength of the velocity fluctuations. In fact, Armistead and Keyes do note that the intensity of pressure fluctuations is roughly two orders of magnitude larger than heat and mass transfer intensities. The overall comparison between the three measures of wall fluctuations (heat and mass transfer and wall pressure) given by Armistead and Keyes (1968a, Fig. 8) does not support their claim of closely related fluctuations of these three measures. Also, the authors' claim for the applicability of wall hot-film probes to detect dynamic wall shear stress using the "demonstrated relationship between mean rate of heat transfer and the wall shear stress" is not verified by their data.

Experiments by Bakewell and Lumley (1967) were conducted to produce large sublayer thicknesses within which data on streamwise velocity fluctuations could be obtained. From the correlations obtained, a flow pattern was proposed which consisted of randomly distributed counter-rotating eddy pairs of elongated streamwise extent (Fig. 3). The authors conclude that this nonlinear vortex stretching mechanism makes invalid earlier suggested theories of linearized sublayer behavior. The implica-

tions of this theory with regard to hot-film response has, to date, not been addressed.

The earlier work of Mitchell and Hanratty (1966) and the theoretical study by Fortuna and Hanratty (1971) overlook the sublayer picture suggested by the model of Bakewell and Lumley. The Hanratty group uses mass transfer techniques operating with very large Schmidt numbers (~5000,

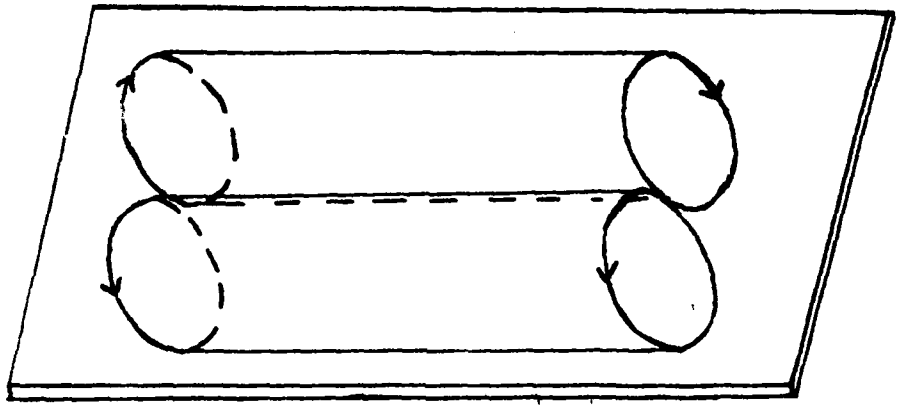

Figure 3. Sublayer model of Bakewell and Lumley (1967).

typically) and it was supposed that the only significant sublayer motions affecting mass transfer in the sublayer were the longitudinal, rectilinear oscillations: they explicitly neglected velocities normal to the flow direction and they also assumed instantaneous longitudinal velocities were linear in distance from the wall.

Later work by Sirkar and Hanratty (1970a,b) acknowledged the importance of the sublayer picture emerging from Bakewell and Lumley's studies since the contribution to time-dependent mass transfer due to longitudinal flow fluctuations is found to be negligible in comparison to that due to velocity gradients in the cross-stream direction and the direction normal to the wall.* In this event, the mass transfer probe cannot be used to measure wall shear stress fluctuations. Kline *et al.* (1967) provide further evidence that the flow in the sublayer is spatially organized, time-dependent large sublayer eddies providing definite regions of updraft and sidedraft, as in Lumley's model, with rather small flow fluctuations in the longitudinal direction.

*This conclusion has yet to be verified!

One question that has been addressed by previous investigators is the following: Is the calibrated relation between hot-film heat transfer and wall shear stress obtained in laminar flow applicable to a turbulent boundary layer? As Pope (1971) points out, the original data of Liepmann and Skinner (1954) were not accurate enough to resolve this question. Pope (1971) derives a correction based on local turbulence intensity that appears to make the laminar and turbulent calibrations coincide; but very limited data are available to test the universality of this correction, and the theoretical basis of the correction appears to be highly questionable. Brown (1967) and Bellhouse and Schultz (1966) find good agreement between laminar and turbulent flow, but the data are very limited. In supersonic external airflow, where laminar sublayers are very thick in comparison with internal flows, Owen and Bellhouse (1970) found good agreement between laminar and turbulent calibrations for the *mean* shear stress as a function of gauge heat loss. No evidence exists regarding the effects of temperature fluctuations on either gauge calibration or the measurement of fluctuating quantities.

Only two examples are known to us of the use of wall gauges to measure the fluctuating component of shear stress. Fortuna and Hanratty (1971), using mass-transfer gauges analogous to heat-transfer gauges, measured the r.m.s. fluctuation in wall shear, τ_w' to be 0.35 $\overline{\tau}_w$. Their measurements were corrected for frequency response as discussed in a previous paragraph. Eckelmann (1974) used a wall-mounted hot-film gauge and measured $\tau_w' = 0.24\ \overline{\tau}_w$. This agreed very closely with the result he obtained by appropriate interpretation of hot-wire velocity measurements. Assuming that the instantaneous velocity profile near the wall is linear, then the instantaneous velocity $\tilde{u}$ and shear stress $\tilde{\tau}$ are related to the instantaneous fluctuations $\tilde{u}'$ and $\tilde{\tau}'$

$$\tilde{u} = \overline{u} + \tilde{u}' \tag{27}$$

and

$$\tilde{\tau} = \overline{\tau} + \tilde{\tau}' \tag{28}$$

He measured the rms velocity fluctuation u' to be 0.24 $\bar{u}$ for values of $y^+ \lesssim 0.1$ (i.e. well within the conventional laminar sublayer boundary of $y^+ = 5$). Therefore, his measurements of u' yield $\tau' = 0.24\ \bar{\tau}$, in agreement with the hot-film result. By an independent method, Popovich and Hummel [(1967a, 1967b); see also Popovich (1969)] obtained $\tau' = 0.30\ \bar{\tau}_w$. A further independent estimate* may be made by combining wall pressure fluctuation data summarized by Leehey (1966) and reported by Blake (1970) with skin friction correlations measured by Burton (1974). The result of this calculation is $\tau'_w = 0.22\ \bar{\tau}_w$.

The measurements of Eckelmann were performed under most favorable conditions; the laminar sublayer of his oil channel was 1 cm thick, 10-100 times thicker than is available with most facilities and sufficiently large that his hot-film wall gauge had a length L^* [see Eq. (13)] of only about 0.03. We expect that the ~ 50% difference between the results of Fortuna and Hanratty (1971) and Eckelmann (1974) arise in part from the supra-linear increase of u' with distance from the wall.

Our research in this area should establish a much firmer foundation for the use of hot-film gauges to measure fluctuations in wall shear stress under a variety of experimental conditions. The fact remains that under normal circumstances the hot-film gauge is subject to cross-stream shear fluctuations as well as streamwise shear fluctuations, and the nature of the gauge response may depend upon the correlation between these two quantities, as suggested by the Bakewell and Lumley (1967) model. The two central questions are: 1) Do three-dimensional effects vitiate the two-dimensional boundary layer assumption that underlies the Reynolds analogy?; 2) Do transient disruptions or distortions of the laminar sublayer so complicate the interpretation of the hot-film gauge performance that its effective use in turbulent applications is precluded? Relevant to both of these questions is the feasibility of developing very simple calibration schemes that properly account for such effects.

In the past decade, a significant fraction of the fundamental research on turbulent boundary layers has been devoted to understanding this

*We are indebted to Prof. P. Leehey of M.I.T. for suggesting this calculation.

bursting phenomenon and integrating these conceptual models with existing data on average and statistical properties of turbulent flows. Well over 100 papers exist on this subject, and it is beyond the scope of the present discussion to treat them in detail. It suffices to note that this is a difficult problem and much research will continue in this area for many years to come. It is clear, however, that both the hot-film gauge and the laser Doppler anemometer are potentially very powerful tools in the continuing investigation of this problem.

B. Theoretical Formulation

The model we are developing is designed to deal with probes of arbitrary geometry, and to account for convection in the fluid and diffusion in all directions in both the fluid and the substrate. The probe is modeled as a heat flux source of arbitrary (but specified) heat flux distribution and geometry located on a plane conducting wall (Fig. 4). The fluid above the probe flows with a uniform shear (i.e., a linear velocity profile*). The governing equations are the three-dimensional fluid and solid energy equations:

$$\nabla^{*2} T_f^* - \frac{s}{\alpha} y^* \frac{\partial}{\partial x^*} T_f^* = 0, \; y^* \geq 0 \tag{29}$$

$$\nabla^{*2} T_s^* = 0, \; y^* \leq 0 \tag{30}$$

*It will be possible to incorporate various other velocity profiles into the model. The linear profile is, however, an excellent assumption for flows in which the thermal boundary layer is much thinner than the momentum boundary layer. Such will be the case for most liquids and for flows in which the thermal boundary layer begins its growth downstream of the beginning of the momentum boundary layer.

where

$$\nabla^{*2} = \frac{\partial^2}{\partial x^{*2}} + \frac{\partial^2}{\partial y^{*2}} + \frac{\partial^2}{\partial z^{*2}},$$

s = fluid velocity gradient ($u^* = sy^*$),

u = fluid velocity in the x direction,

T = temperature measured above ambient,

α = fluid thermal diffusivity,

*: denotes dimensional quantities,

f: as a subscript denotes fluid quantities, and

s: as a subscript denotes solid (substrate) quantities.

The temperature field is continuous at the fluid-solid interface. The heat flux is also continuous at this interface, except at the probe which acts as a source of heat. Thus:

$$T_f^* = T_s^* \quad \text{at } y^* = 0 \tag{31}$$

$$k_s \frac{\partial T_s^*}{\partial y^*} - k_f \frac{\partial T_f^*}{\partial y^*} = Q^*(x^*, z^*) \text{ at } y^* = 0 \tag{32}$$

where k is the thermal conductivity and Q^* is the arbitrary (but specified) probe heat flux distribution. At sufficiently large distances from the probe, the temperature must attain the ambient value, or

$$T_f^*, T_s^* \to 0 \text{ as } x^*, y^* \text{ or } z^* \to \pm \infty \tag{33}$$

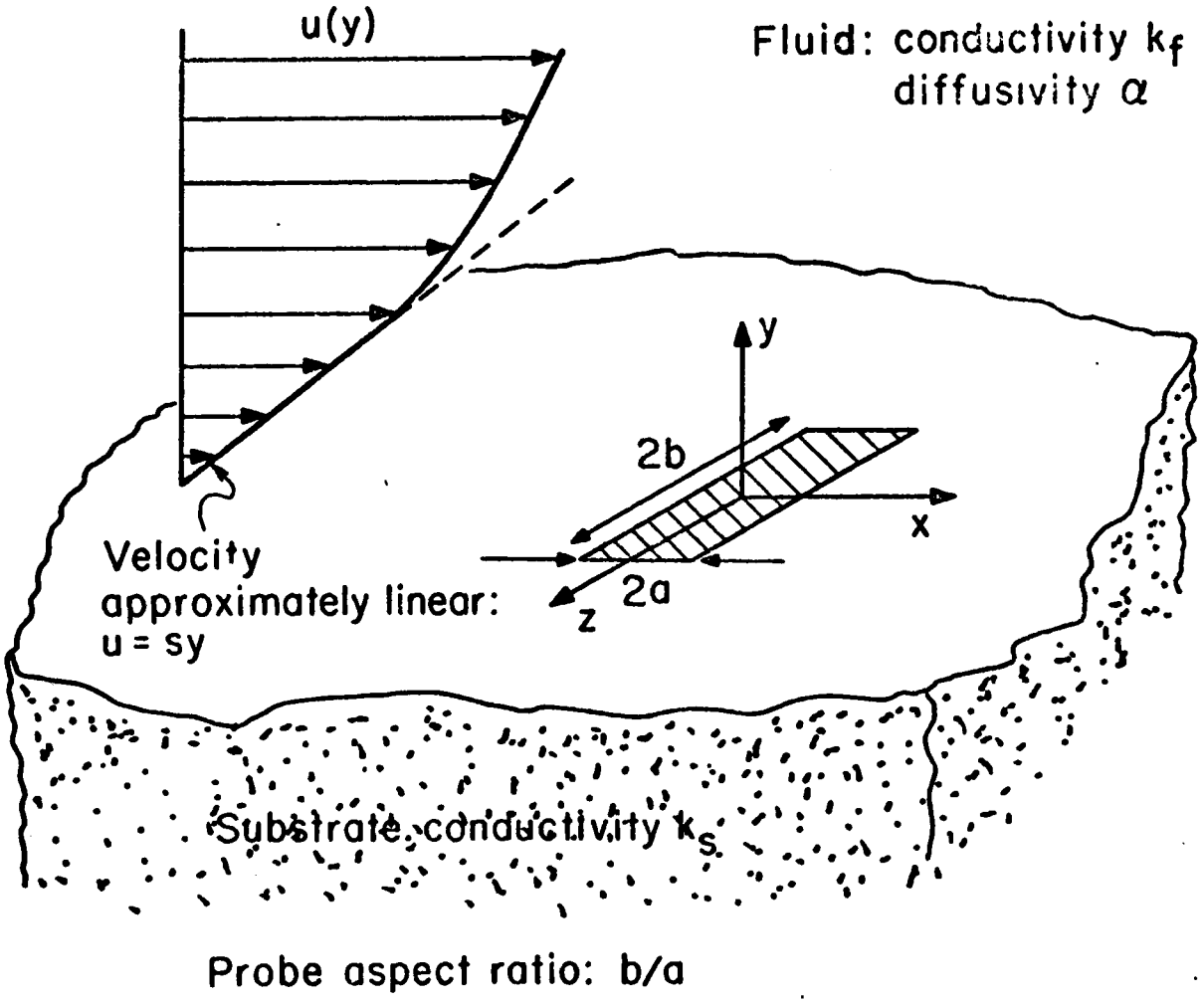

Figure 4. Schematic View of a Rectangular Hot-Film Probe and Its Environment.

These equations can be cast in a form more amenable to analysis by appropriate nondimensionalization. We define

$L \equiv \sqrt{\alpha/s}$ a characteristic length for thermal diffusion

$P_s \equiv$ the total power output of the probe $\left(= \int_{-\infty}^{\infty}\int_{-\infty}^{\infty} Q^* \, dx^* \, dz^*\right)$

and introduce dimensionless quantities:

$$x = x^*/L, \; y = y^*/L, \; z = z^*/L$$

$$T = T^* \, k_f L/P_s$$

$$K = k_s/k_f$$

$$Q(x, z) = Q^*(x^*, z^*) \cdot L^2/P_s.$$

Equations (29)-(33) can now be expressed as:

$$\nabla^2 T_f - y \frac{\partial T_f}{\partial x} = 0, \quad y \geq 0 \tag{34}$$

$$\nabla^2 T_s = 0, \quad y \leq 0 \tag{35}$$

$$T_f = T_s, \quad y = 0 \tag{36}$$

$$K \frac{\partial T_s}{\partial y} - \frac{\partial T_f}{\partial y} = Q(x, z), \quad y = 0 \tag{37}$$

$$T_f, \; T_s \to 0 \quad \text{as } x, y, z \to \pm \infty \tag{38}$$

The solution of Eqs. (34) - (38) depends on only the conductivity ratio K and the source distribution $Q(x, z)$. The shear s is part of the definition of a characteristic diffusion length ($L \equiv \sqrt{\alpha/s}$). A flow Peclet number can be obtained from the definition of Q: for a characteristic streamwise probe dimension of length L_p^*, the Peclet number is $SL_p^{*2}/\alpha = (L_p^*/L)^2$.

Equations (34) - (38) represent a general model for analyzing hot-film probes in steady uniform shear flows. We are developing an efficient and flexible solution procedure for this set of equations which retains all terms of the equations, allows for all ranges of the values of the governing parameters, and permits the specification of arbitrary probe geometries and heat fluxes (i.e., arbitrary $Q(x, z)$, including the analysis of multiple-film probes. Solution of this system of equations yields a relation between probe heat flux and the resulting temperature field. A numerical "calibration" of a probe design is then made possible by knowledge of the relations between fluid shear, probe temperature, and probe heat flux.

Method of Solution

The temperature field at $y = 0$, $T_o(x, z)$, is obtained from our model [Eqs. (34) - (38)] by a combination of analytical and numerical techniques. Solving for the temperature field at only one value of y ($y = 0$, here) greatly increases computational efficiency. Solutions to the energy equations in both the fluid [Eq. (34)] and solid [Eq. (35)] domains are obtained by first analytically performing Fourier transforms in both the streamwise and spanwise directions. These two-dimensional transformations reduce the partial differential equations (34) and (35) to ordinary differential equations whose solutions are then found. The arbitrary constants of these solutions are evaluated from the Fourier transforms of the boundary conditions [Eqs. (36) - (38)]. This method of solution is similar to that used by Tanner [1967] and by Davies and Kimber [1972] in solving simplified forms of the governing equations.

The two-dimensional Fourier transform of the wall temperature distribution is defined as

$$\hat{T}_o(p, q) = \int_{-\infty}^{\infty} \int_{-\infty}^{\infty} e^{2\pi i(px + qz)} T_o(x, z)\, dxdz . \qquad (39)$$

We have found the solution of Eqs. (34) - (38) in two-dimensional transform space to be:

$$\hat{T}_o\,(p,\,q) = \hat{Q}\,(p,\,q)\,\frac{e^{\pi i/6}}{(2\pi p)^{1/3}}\,\frac{Ai(\Omega)/Ai'(\Omega)}{K\Omega^{1/2}\,Ai(\Omega)/Ai'(\Omega) - 1} \tag{40}$$

$$\Omega = e^{\pi i/3}\,(2\pi)^{4/3}\,\frac{p^2 + q^2}{p^{2/3}}$$

where

$A_i(\Omega)$ = the Airy function of complex argument Ω,

$Ai'(\Omega) = \frac{d}{d\Omega}\,(Ai(\Omega))$,

p = transform variable in the x direction,

q = transform variable in the z direction, and

$\hat{Q}$ = the two-dimensional transform of Q.

The desired temperature field, $T_o\,(x,\,z)$, is then found by application of the two-dimensional inverse Fourier transform:

$$T_o\,(x,\,z) = \int_{-\infty}^{\infty}\int_{-\infty}^{\infty} e^{-2\pi i\,(px\,+\,qz)}\,T_o\,(p,\,q)\,dpdq\,. \tag{41}$$

All of the information specifying the details of the probe geometry and its heat flux distribution is contained in $\hat{Q}\,(p,\,q)$. The analyses of most other researchers can be viewed as special cases of this solution. For example, an adiabatic wall solution is obtained by setting the conductivity ratio K to zero. A two-dimensional geometry can be analyzed by making the heat flux distribution $Q\,(x,\,z)$ very much longer

in the spanwise direction than in the streamwise direction.

The complexity of the integrand (40) of inversion integral (41) necessitates a numerical evaluation. The inversion is achieved by applying a series of numerical one-dimensional Fast Fourier Transforms (FFT's) first in one direction and then in the other. The integrand (40) to which the FFT's are applied must first be evaluated numerically at a finite set of discrete values of (p, q). The Airy function and its derivative are evaluated from series expansions. Taylor series are used for small values of $|\Omega|$, and asymptotic series are used for larger values of the argument. The transform of the heat flux source distribution, $\hat{Q}$ (p, q), can be found analytically for relatively simple source distributions (e.g., uniform flux over a rectangular probe), and can be obtained numerically for more complicated distributions. All operations are performed using complex arithmetic.

The numerical evaluation of Eqs. (40) and (41) is currently under development. The initial cases being investigated include a point source of heat mounted on an adiabatic wall and a square uniform heat flux probe exposed to a moderate Peclet number flow and mounted on a wall of variable conductivity. Preliminary calculations of the wall temperature distributions along x = 0 and along z = 0 for a square uniform heat flux probe mounted on a adiabatic wall at a Peclet number of 36 are shown in Fig. 5. These calculated distributions are qualitatively reasonable: along z = 0 the peak temperature occurs above the probe but downstream of its midpoint, the temperature distributions decay monotonically in all directions from the maximum value, and the streamwise temperature profiles are skewed such that the downstream decay is much slower than the upstream decay. The spanwise temperature profiles, as expected, are symmetric about z = 0.

Streamwise (z = 0) temperature profiles for a square uniform heat flux probe mounted on an adiabatic wall at Peclet numbers ranging from 4 to 64 are presented in Fig. 6. Here, the temperature profiles are normalized by multiplying by the probe length, L_p. The point of maximum temperature moves further upstream with increasing Peclet number. As the Peclet number increases, the decay of the temperature distributions

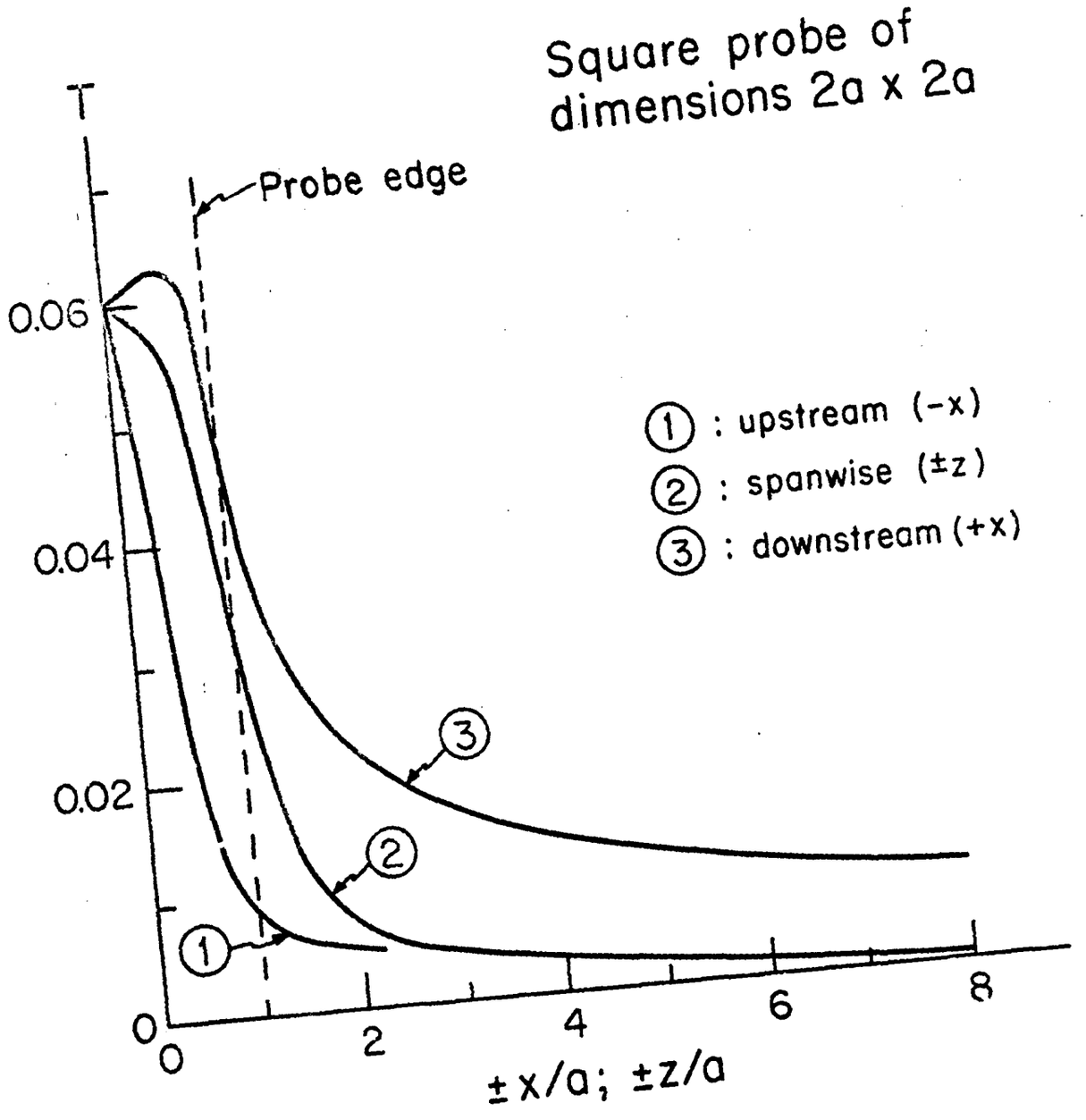

Figure 5. Predicted Upstream, Downstream, and Spanwise Temperature Profiles for a Square Probe; K=0; Pe=36.

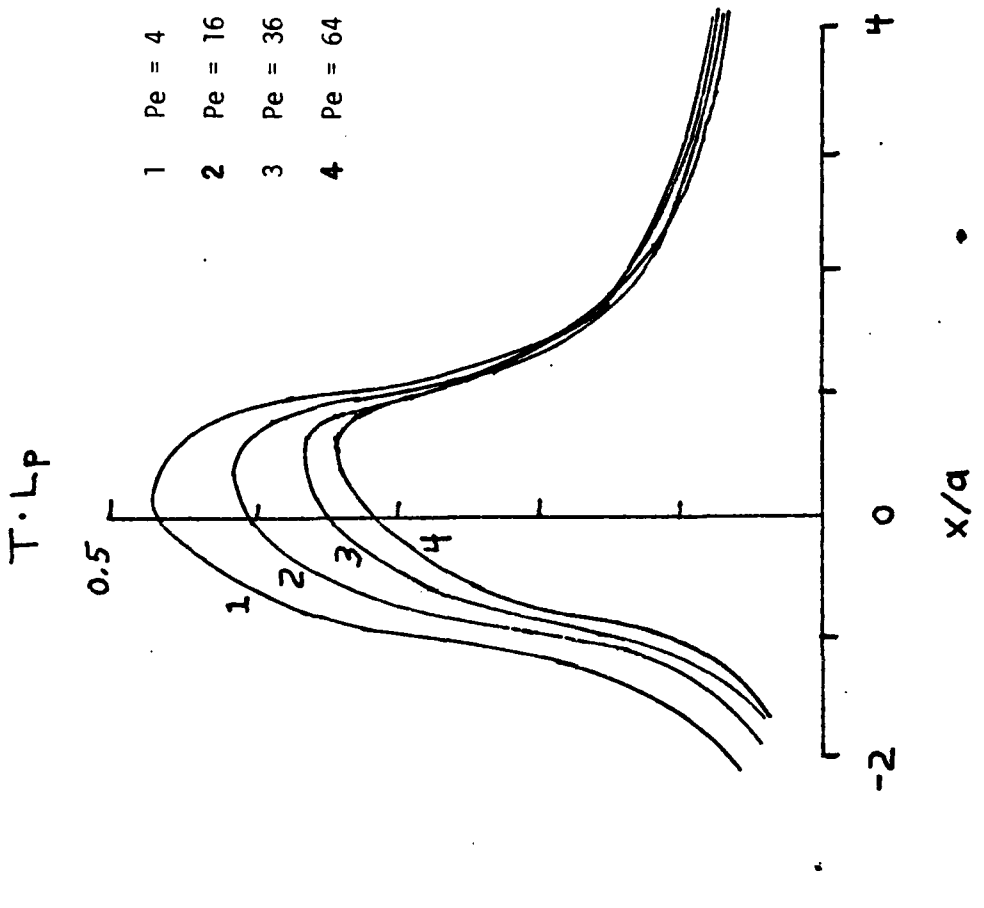

Figure 6. Effect of Varying Peclet Number on Streamwise Temperature Profiles for a Square Probe; K=0. (Lp=2a).

proceeds less rapidly downstream and more rapidly upstream. The average probe temperature is also seen to decrease with increasing Peclet number (indicating a probe heat transfer rate per unit average temperature that increases with Peclet number). The effect of varying conductivity ratio on the streamwise ($z = 0$) temperature profiles due to a square uniform heat flux probe at constant Peclet number (here Peclet number equals 16) is presented in Fig. 7. Increasing the conductivity ratio results in calculated temperature profiles that are lower in magnitude, whose maximum move closer to the probe center, and that are more symmetric about these maximums.

That the calculated temperature distributions have not decayed to zero results from the use of a discrete rather than continuous transform. This results in a truncation of the physical space computational domain. Another possible source of error in the computed results is the use of a finite rather than infinite transform. Tests are being conducted to determine the discretization and truncation which will introduce negligible error in the computed temperature distributions. An appropriate average integrated value of the integrand at $(p, q) = (0, 0)$ has been found to deal with the singularity there.

C. Continuing Research

Testing and refinement of our computational model is currently in progress. We are generating solutions for simple probe geometries and flow situations to be checked against existing analytical and numerical solutions and available experimental data. After this initial verification and refinement, we will investigate more complicated probe and flow geometries with the dual goal of gaining a better understanding of the complicated heat transfer processes involved and of conducting parametric probe design studies. Such analyses will enable us to provide a "numerical calibration" of a probe design. Experimental work utilizing hot-film probes for shear stress measurement in both steady and unsteady flows has been in progress in our laboratory for some time. A future stage of our experimental effort will be to fabricate probes of different geometries and substrate

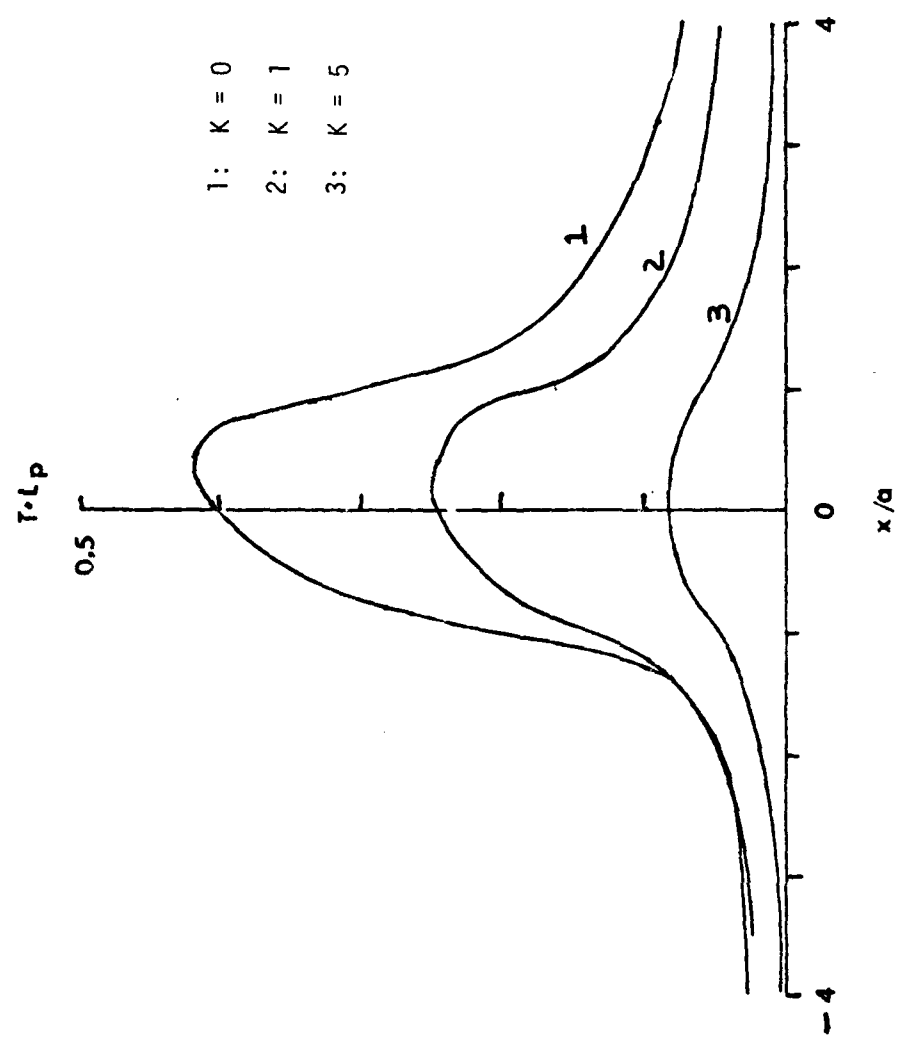

Figure 7. Effect of Varying Conductivity Ratio on Streamwise Temperature Profiles for a Square Probe; Pe=16. (Lp=2a).

conductivities which have been designed by our computational model. These can then be tested under a variety of flow conditions enabling us to verify our "numerical calibrations" and to gain additional understanding of the underlying physics. Our steady flow model and experiments should also provide much needed insight into the performance of probes in unsteady flows.

III. LASER DOPPLER ANEMOMETRY

A. Review of Literature

The laser Doppler anemometer (LDA) has undergone extensive development in the past decade and is now a versatile and accurate instrument for measuring velocities with minimal disturbance to the fluid flow under investigation. Several excellent monographs on the theory and operation of the LDA are available [Durst, Melling and Whitelaw (1976), Durrani and Greated (1977)]; and a recent review paper [Buchave, George and Lumley (1979)] describes the state of the LDA art in the measurement of turbulence.

The LDA optical configuration that is now used most frequently is termed the "differential Doppler" or "fringe" mode of operation; it is illustrated in Figure 8. Two intersecting laser beams form an interference

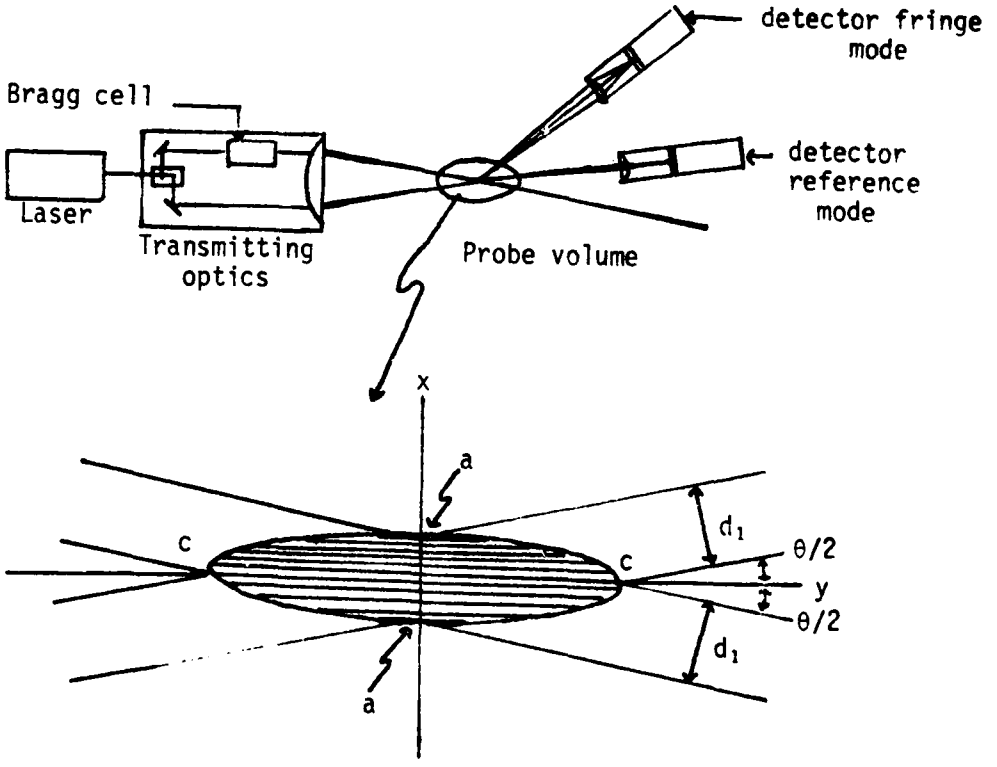

Figure 8. Geometry of the LDA fringe mode configuration. An explanation of the symbols appears in the text. [After Buchave *et al.* (1979)].

fringe pattern in the fluid that is orthogonal to the component of velocity to be measured. In the absence of a Bragg cell frequency shifter, this fringe pattern is stationary. Any small particle that passes through the fringe pattern will scatter light, producing a signal at the detector with a frequency proportional to the particle velocity normal to the fringes and inversely proportional to the fringe spacing.

If the fringes are stationary, the detector will not distinguish between particles moving in opposite directions with the same velocity. By introducing a Bragg cell in one of the optical paths, the beams can be made to have slightly different frequencies and the resultant fringe pattern will be a moving one, the fringes continuously sweeping across the probe volume in one direction. The scattered light signal from a particle moving through the probe will now be sensitive to the direction of the particle motion. A further refinement is the use of multi-colored or polarized beams and additional detectors to measure, simultaneously, two or three components of the particle velocity.

It is not our intention to present here a comprehensive review of the experimental challenges that arise in the many and varied applications of LDA instrumentation. We propose to study, compare, and calibrate against each other, two methods of measuring wall shear stress in unsteady and turbulent flows; and we discuss here only those factors of LDA operation that are most important in this context.

The way in which the LDA can be used to determine wall shear stress is conceptually straight-forward. The two orthogonal components of fluid velocity parallel to the surface of a wall are measured with the LDA at a series of locations above the surface. If (x, z) are the coordinates in the plane of the surface and (u, w) are the velocities in these directions, then the magnitude of the surface vector shear stress for a Newtonian fluid is

$$\overline{\tau}_w = \left[\left(\overline{\mu \frac{\partial u}{\partial y}} \right)_w^2 + \left(\overline{\mu \frac{\partial w}{\partial y}} \right)_w^2 \right]^{1/2} , \qquad (42)$$

where y is measured normal to the surface and $(\partial u/\partial y)_w$ and $(\partial w/\partial y)_w$ are

the measured velocity gradients at the wall.

The accurate determination of $\overline{\tau}_w$ and the fluctuating shear stress τ_w' require a careful assessment of potential errors and the use of appropriate corrections to the raw measurements. These corrections, summarized by Buchhave *et al.* (1979), include the following:

> (1) A correction for spurious frequency components arising from the entry and exit of individual particles from the measuring volume. This term is referred to as "transit time broadening"; it is not present when the so-called "burst mode" or single-particle analysis is used.
>
> (2) A correction for bias arising from the presence of velocity gradients across the measuring volume (gradient broadening").
>
> (3) A correction to account for the phase fluctuations arising from correlation of the light scattered from several particles within the measuring volume ["turbulence broadening"; see George and Lumley (1973)].

In addition to these calculable and correctable sources of broadening, the experimenter is faced with the necessity of achieving good spatial resolution, designing a stable and repeatable optical system that can traverse a region of high shear with an accuracy of a few μm, and having a collection system for the scattered radiation that exhibits a very high signal-to-noise ratio. The system we propose to use has these attributes. To understand the advantages of the system we propose, a review of previous experiments is necessary.

Table 1 presents the conditions of measurement of the seven previous published experiments we consider most relevant to our proposed research. Of these, the measurements of Karpuk and Tiederman (1976) and Quigley and Tiederman (1977) are the most successful in achieving good spatial resolution near the wall of a turbulent flow. These excellent experiments were able to provide confirmation of certain of the correction factors predicted by theory [see the summary of Buchhave *et al.* (1979)] that were described in the previous paragraph. The authors demonstrate that, even under *favorable* circumstances, uncorrected LDA signals will yield apparent mean velocities 10-30% greater than the true mean; and measured rms fluctuations may be in

Table 1. LDA Measurements Near Solid Surfaces

Investigators	LDA Mode and Detection	Effective Probe Vol. Dimensions (μm)	Est. B.L. Thickness, $y^+ = 5$ (μm)	Comments
Berman & Dunning (1973)	Ref. beam mode Multiple particle Frequency demodulator	2a ≈ 17 to 113 2c ≈ 60 to 1600	~250 μm	Measurements not made closer to wall than $y^+ = 25$. Correction for various broadening mechanisms.
Oldengarm *et al.* (1975)	Fringe mode Forward scattering Multiple particle Spectrum analyzer	2a ~ 8 μm 2c ~ 35 μm	~ 60 μm Laminar flow	Spectrum showing transit time broadening @ y = 13.6 μm and y = 95 μm
Karpuk & Tiederman (1976) Quigley & Tiederman (1977)	Fringe Mode Side scattering Single particles Burst processing	Cylindrical; parallel to wall 2c = 61 μm 2b = 244 μm	~250 μm	Correction for bias arising from velocity gradient.
Agrawal *et al.*	Fringe mode Forward scattering Multiple particles Frequency Tracking	2a = 45 μm 2c = 256 μm	~2000 μm* Laminar	Primary emphasis on velocity profiles across entire pipe. Curved pipe with secondary flow.
Born *et al.* (1978)	Fringe mode Backscatter Multiple particles Frequency tracker	2a ~ 10 μm 2c ~ 18 μm	~40 μm* Laminar	Blood flow in 200 μm tube. Measurement of broadening.
Reich (1978)	Fringe mode Forward scattering Multiple particles Frequency tracker	2a ~ 100 μm	<< 10^3 μm*	Turbulence near a membrane. Beams parallel to surface.
Yoganathan *et al.* (1979)	Fringe mode Forward scattering Multiple particles Frequency tracker	2a = 120 μm 2c = 720 μm	~100 μm*	Beam volume strongly overlapped wall and sublayer.

*Estimated region of maximum gradient. The criteria $y^+ = 5$ does not have a useful correlation with the region of maximum velocity gradient in laminar flow.

error by 100% or more*. After appropriate correction, they obtain values of $\bar{\tau}_w$ that are in agreement with pressure drop measurements and values of $(\tau'_w/\bar{\tau}_w)$ at $y^+ = 2$ that are in substantial agreement with the careful measurements of Eckelmann (1974) that were cited in a previous section.

The experiments of Reich (1978) and Oldengarm *et al.* (1975) are somewhat qualitative, inasmuch as Reich fails to account for significant transit time broadening and Oldengarm *et al.* make no attempt to correct their measurements for bias arising from gradient broadening. Agrawal *et al.* (1978) were concerned with skewed laminar flow in curves tubes, and no attempt was made to make detailed measurements near the tube walls; furthermore, their laminar flow had much less severe velocity gradients than generally occur in turbulent or highly unsteady flows. As far as the experiments of Yoganathan *et al.* (1979) are concerned, they made no effort to quantify the errors of their measurements; we calculate that their reported wall shear stresses are potentially in error by a substantial amount.

We now turn to the question of signal-to-noise ratio of the scattered radiation received by the detector. A careful examination of various alternative optical arrangements has convinced us that the backscatter arrangement, as used by Born *et al.* (1978) and others, is by far the most useful for measurements near solid surfaces. The angle θ between the two intersecting beams must be large to achieve small probe volume dimensions; and this allows relatively large collection angles for the backscattered radiation, thereby increasing the amount of received signal.

One formidable difficulty in all LDA measurements near surfaces is that imperfections in the surface itself will cause unwanted scattered radiation to be collected by the detector. This background signal is frequently very large compared to the amount of radiation scattered by a

*This is consistent with the large errors in mean velocity observed by Born *et al.* (1978) near the wall of a small tube, although the corrections Born *et al.* compute are in error. Their Eq. (2) contains several misprints [compare, e.g. Berman and Dunning (1973)]. Further, their computed correction does not agree with the proper relation of Berman and Dunning.

moving particle in the fluid. An example of how this background scattering can dominate the detector signal is given by the results of Oldengarm *et al.* (1975). Normally high-pass electronic filters are used to reduce the magnitude of this background, but such electronic discrimination is marginal at best and cannot remove the photocurrent shot noise that contributes to the filtered signal.

An elegant method of removing these large background signals was proposed by Stevenson *et al.* (1975). They used test particles containing fluorescent dye. As the test particles traverse the measuring volume, the incident laser light is absorbed and reradiated as fluorescent emission at longer wavelengths. Inasmuch as the fluorescent lifetime of suitable dyes is on the order of 1-10 nsec, the fluorescent intensity is directly proportional to the instantaneous fringe field intensity experienced by the measuring particle.

Laser-induced fluorescence therefore shifts the signal radiation to longer wavelengths, allowing the use of simple optical filters to remove all unwanted scattered light at the excitation wavelength. In the backscatter mode, the fluorescence signal is comparable to that which would be produced by ordinary particle scattering.

Although the use of fluorescence rather than scattering has many obvious advantages, particularly for backscatter systems, no reports of the use of this technique have appeared in the literature since the original publication of Stevenson *et al.* in 1975. Private communication with Dr. T. Powell of NASA-Lewis and Dr. Carl Williams of United Technology Research Laboratories have confirmed that the fluorescence method exhibits the advantages cited previously. However, they have encountered one practical difficulty with the method described by Stevenson *et al.*, a difficulty that our system will avoid.

Stevenson *et al.* (1975) produced fluorescent particles by atomizing liquids containing appropriate fluorescent dyes. These liquid droplets are suitable for air flows but are unsuitable for measurements in liquids. Even in gas streams, the droplets tend to impinge on surfaces, leaving a fluorescent residue on the surface that produces background signals similar

to those caused by wall imperfections in conventional scattering systems. According to Williams (private communication), this prohibits the use of the fluorescence method within 3-4 probe volumes of the surface.

Our research will employ solid particles containing fluorescent dye, thereby eliminating entirely the difficulties encountered with the liquid droplet system used by Stevenson and others.

In summary, a backscatter LDA system using fringe-mode single-particle detection is found to be superior to other optical arrangements for velocity measurements near solid surfaces. The use of solid fluorescent particles will eliminate the large background signals that have characterized previous experiments using scattered laser light and liquid fluorescent particles.

B. System Design

The operation of the laser Doppler velocimeter in the "fringe mode" is based on fairly simple concepts. If two coherent, linearly polarized laser beams are brought to a focus at a common point, a set of intensity fringes is produced at the beam intersection. These fringes are equally distant from each other; their spacing can be calculated from the geometry of the optical train. A particle traversing this field of spatially varying light intensity scatters light with an intensity proportional to that of the incident laser intensity. The scattered light is collected by a photodetector and the signal is transmitted to a counter. The counter clocks the time taken by the particle to cross the fringes and simultaneously determines the frequency of crossing. The particle velocity perpendicular to the fringe planes is calculated by taking the product of the frequency and the fringe spacing.

In order to complete a quantitative analysis of the laser scattering process, it is necessary to describe at some length the fringe field produced by two focused, intersecting, coherent laser beams. The following sections explain the interference phenomenon, the nature of Gaussian beams, and the details of the region produced by the intersection of the laser beams. Tracer particles are then selected for their abilities to follow the flow and produce a satisfactory signal. The concluding section of

this chapter describes the shot noise associated with background scatter.

Interference and Fringe Spacing

When two light beams originating from the same source are superimposed, interference results. This phenomenon of interference is characterized by intensity variations where the maxima may exceed the linear sum of the intensities of the two beams and where the minima may be zero. In the case of plane, monochromatic, linearly-polarized light waves, this interference is seen as a series of bright and dark fringes which represent regions of maximum and minimum intensity, respectively.

The output of a laser can be ideally described as a plane, monochromatic, linearly-polarized light beam. In LDA, the output beam is split by means of an optical beamsplitter into two beams, each with a lower intensity than the original beam. The two resulting beams are subsequently intersected with one another to form a region of interference that is characterized by a series of bright and dark intensity fringes.

Figure 9 depicts two such beams, represented by electric field vectors ε_1 and ε_2, intersecting. ζ_2 and η_2 represent the directions of propagation, and the lines orthogonal to these directions represent the locations of a crest or a peak in the wave. ε_1 and ε_2 can be expressed as complex, scalar quantities; the scalar representation arises because both beams are not only plane and monochromatic, but linearly polarized.

$$\varepsilon_1 = (E_0)_1 \exp\left[i(2\pi\nu t - \kappa\eta_2 + \phi_1)\right] \tag{43a}$$

$$\varepsilon_2 = (E_0)_2 \exp\left[i(2\pi\nu t - \kappa\zeta_2 + \phi_2)\right] \tag{43b}$$

In the above equations, $(E_0)_i$ represents the amplitude of the electric field vector for the $i^{\underline{th}}$ beam, κ represents the wave number and equals $2\pi/\lambda$, and ϕ_i represents the phase of the $i^{\underline{th}}$ beam. The total

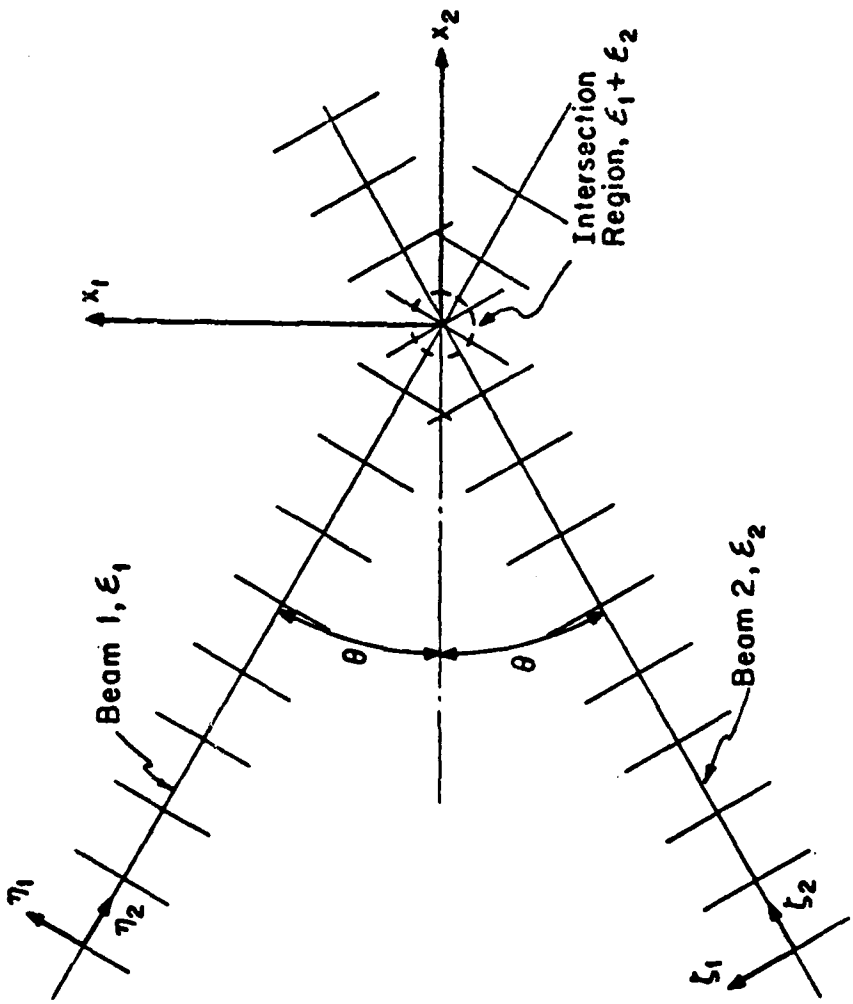

Figure 9. Intersection of Two Plane, Monochromatic, Linearly-Polarized Light Beams. ε_1 and ε_2 Represent Electric Field Vectors.

electric field in the intersection region can be expressed as:

$$\varepsilon = \varepsilon_1 + \varepsilon_2 \tag{44}$$

The intensity variation across the region is given by the time average of the square of the electric field, where the time average is taken over a large interval of time compared with the period, $2\pi/\nu$. The following expression is obtained for intensity (Durst, Melling, and Whitelaw, 1976):

$$I = (E_o)_1^2 + (E_o)_2^2 + 2(E_o)_1(E_o)_2 \cos\left[\frac{2\pi}{\lambda}(\zeta_2 - \eta_2) + (\phi_1 - \phi_2)\right] \tag{45}$$

Assuming that the phases of the beams are equal to each other at t = 0, the maximum intensity occurs when $(\zeta_2 - \eta_2) = N\lambda$, or at an integral number of wavelengths. The minimum intensity occurs when $(\zeta_2 - \eta_2) = (N + \frac{1}{2})\lambda$.

Figure 10 depicts an enlarged view of the interference region where the dark horizontal lines represent the intersections of the crests in the beams. The fringe spacing can be calculated with the aid of this diagram and a coordinate transformation. From the geometry in Figure 10.

$$\eta_2 = x_2 \cos\theta - x_1 \sin\theta$$

$$\zeta_2 = x_2 \cos\theta + x_1 \sin\theta$$

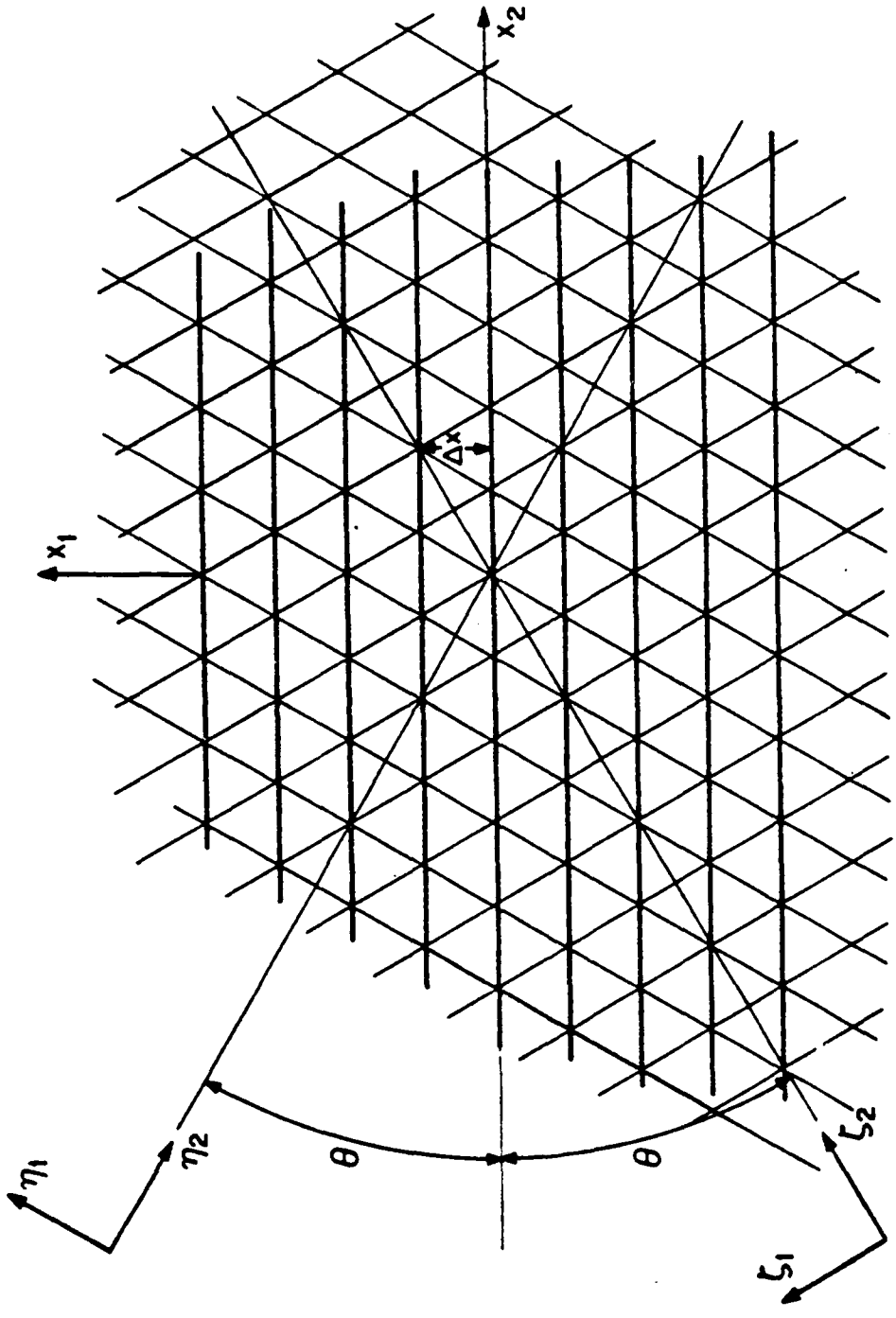

Figure 10. Formation of Fringes in Interference Region. Crossing Angle of Beams = 2θ.

where θ is the half-angle of intersection. Subtracting η_2 from ζ_2 gives:

$$(\zeta_2 - \eta_2) = 2x_1 \sin\theta$$

the $N^{\underline{th}}$ fringe is given by:

$$(\zeta_2 - \eta_2) = N\lambda = 2(x_1)_N \sin\theta$$

and the $(N + 1)^{\underline{th}}$ fringe by:

$$(\zeta_2 - \eta_2) = (N + 1)\lambda = 2(x_1)_{N+1} \sin\theta$$

Hence,

$$(x_1)_N = \frac{N\lambda}{2 \sin\theta} \; ; \; (x_1)_{N+1} = \frac{(N+1)\,\lambda}{2 \sin\theta} \tag{46}$$

and the distance between the two fringes, d_f, is:

$$d_f = \Delta x = (x_i)_{N+1} - (x_1)_N = \frac{\lambda}{2 \sin\theta} \tag{47}$$

Thus, the fringe separation is dependent only on the wavelength of the intersecting beams and the angle at which they intersect.

Rudd's Fringe Model

The principle of the interference fringe model proposed by Rudd in 1961 [see Durst et al. (1976)] provides a clear physical insight into the physics of LDA and a quantitative basis for analyzing laser Doppler signals. A particle passing through a set of interference fringes, as seen earlier in Figure 10, scatters light with an intensity proportional to that of the

light incident upon it. The scattered light is detected by a photomultiplier which converts the incoming optical signal into an electrical signal. The electrical signal is passed on to an electrical counter which calculates the frequency of crossing, ν_D. This signal frequency is related to the velocity of the particle in the direction perpendicular to the fringe planes, V_x, by the following equality:

$$\nu_D = \frac{V_x}{d_f} = \frac{2V_x \sin\theta}{\lambda} \tag{48}$$

where d_f was calculated in Equation (47).

ν_D is commonly referred to as the Doppler frequency, although when speaking in terms of Rudd's fringe model the term Doppler frequency is not quite accurate. The above expression for ν_D, however, is the same as that obtained for the signal frequency based on Doppler considerations (Durst, Melling, and Whitelaw, 1976). The semantics problem of whether or not the fringe system just described can justifiably be called a Doppler system is not of practical interest. Further reference to the Doppler anemometer and the Doppler frequency, ν_D, will be understood to comprise the above mentioned fringe system and signal frequency, respectively.

Gaussian Beams

In LDA systems the laser is almost always operated in the TEM_{00} (fundamental transverse electromagnetic) mode resulting in a beam with a Gaussian intensity profile. Figure 11 depicts such a Gaussian beam with a beam waist of $2w_0$, a beam radius of $w(z)$ at some arbitrary z-location, and plane wavefronts with radius of curvature, $R(z)$. The beam waist, which is the narrowest portion of the beam, and the beam radius, $w(z)$, are defined at the $1/e^2$ intensity points. $w(z)$ is given by:

$$w^2(z) = w_0 2 \left[1 + \left(\frac{\lambda z}{\pi w_0}\right)^2\right] \tag{49}$$

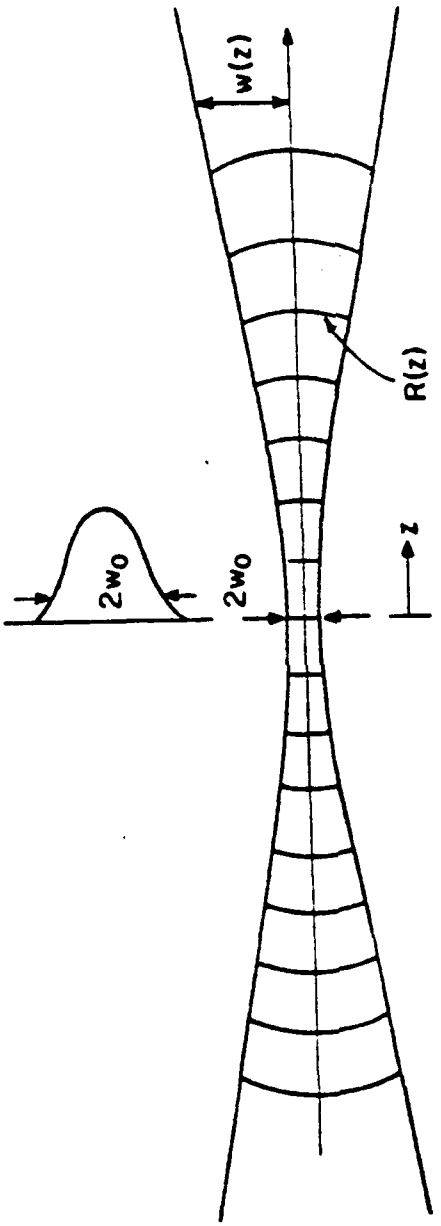

Figure 11. Profile of a Gaussian Beam.

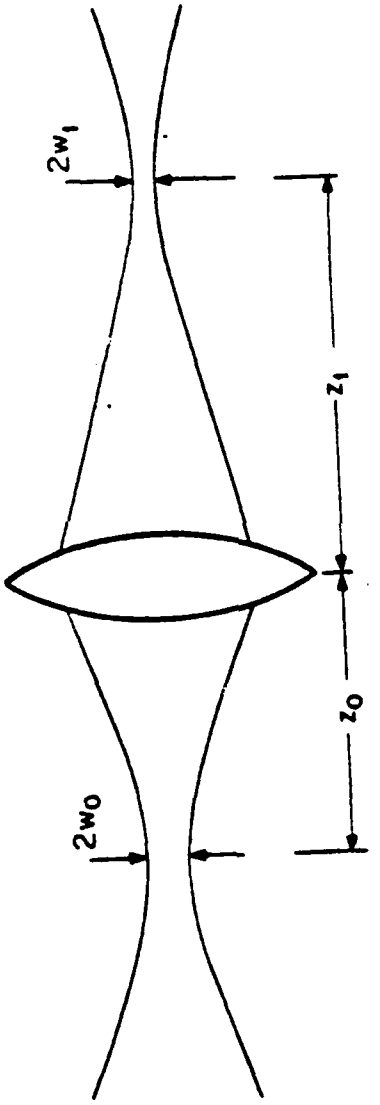

Figure 12. Gaussian Beam After Focusing By a Lens.

The radius of curvature, R(z), of the wavefront can be computed:

$$R(z) = z \left[1 + \left(\frac{\pi w_o^2}{\lambda z}\right)^2\right] \tag{50}$$

From this equation it is seen that at z = 0, R(z) goes to infinity and the wavefronts are essentially planar.

The original size and location of the beam waist is determined by the configuration of the laser cavity. The size and location of the beam waist after being focused by a lens (see Figure 12) are given by:

$$z_1 = f + \frac{(z_o - f)f^2}{(z_o - f)^2 + \left(\frac{\pi w_o^2}{\lambda}\right)^2} \tag{51}$$

$$w_1 = \frac{w_o f}{\left[(z_o - f)^2 + \left(\frac{\pi w_o^2}{\lambda}\right)^2\right]^{1/2}} \tag{52}$$

where f is the focal length of the lens. Hence the focused beam waist is generally not located in the front focal plane of the lens. The exceptional case occurs when z_o is in the back focal plane.

When two Gaussian beams are focused by a lens of focal length f, the volume circumscribed by the $1/e^2$ intensity points of the fringes is called the probe volume. Since the beam waists are not found at the front focal plane of the lens (except when $z_o = f$) they do not intersect at the center of the probe volume and may even be outside the probe volume. In either case some, if not all, of the wavefronts within the probe volume will have a finite radius of curvature and will exhibit a varying fringe spacing as shown in Figure 13. This results in signals of varying frequencies depending on the path traversed by the particle through the probe volume. Durst and

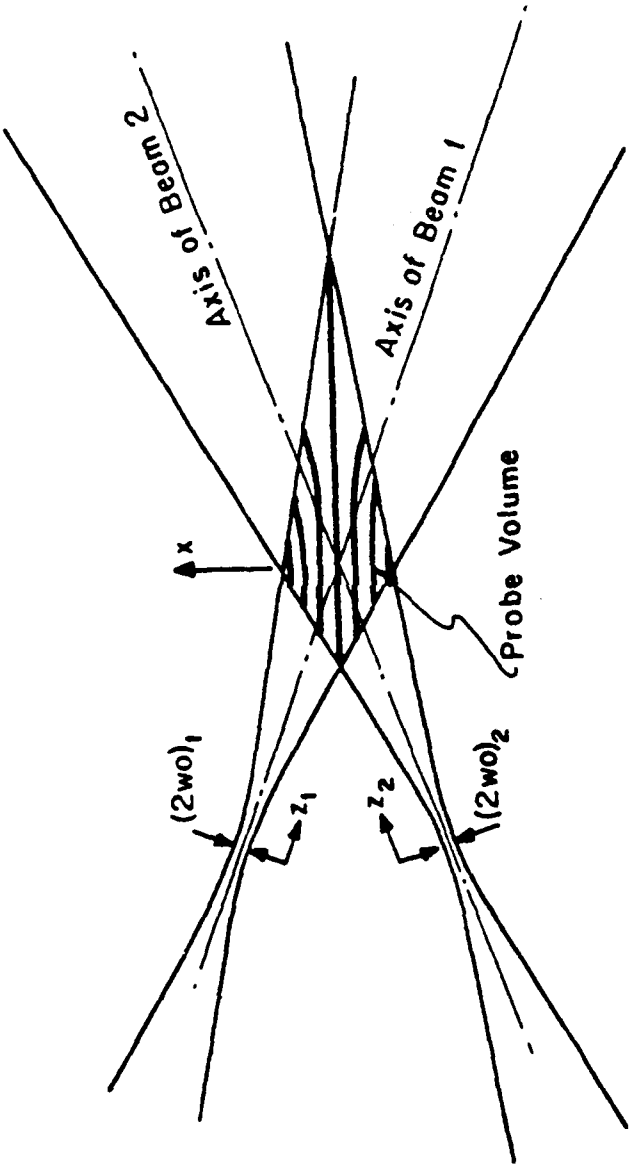

Figure 13. Distortion of Fringes Due to Improper Intersection of Gaussian Beams.

Stevenson (1979) found the gradient of the Doppler frequency along the probe volume to be

$$\frac{f}{\nu_D}\left(\frac{d\nu_D}{dz}\right) = \frac{(z_o - f)}{f} \tag{53}$$

To assure that the waists of both beams intersect, an additional optical component consisting of both a positive and a negative lens is positioned between the laser and the transmitting lens. The position of the beam waists relative to the lens can then be varied and made to occur at the front focal plane of the lens.

Calculation of Probe Volume Dimensions

If the beam waists do intersect after being focused by a lens, an elliptical probe volume is formed. The dimensions of this probe volume are determined by the geometry of the optical system.

Figures 14 and 15 depict a fairly complicated set-up consisting of two beams expanded in air and subsequently focused by two lenses into a medium with an index of refraction different from that of air. Figure 14 is a side view of the set-up; consequently only one of the beams is seen. Figure 15 illustrates the position of the other beam relative to the first. The result is an ellipsoid consisting of a set of parallel fringe planes equally distant from one another. The diameter, d_m, length, ℓ_m, and width, w_m, can be calculated given i, r_o, d_{bo}, ex, f_1, f_2, ℓ, and z, where:

i = index of refraction of medium

r_o = distance between beams and optical axis

d_{bo} = diameter of beams entering beam expander (assumed to be diameter leaving laser)

ex = beam expansion ratio

f_1, f_2 = focal lengths of lenses 1 and 2, respectively

ℓ, z_1 = variable distances representing locations of lens 2 and medium's boundary with respect to lens 1

In Figure 14, the beams enter the beam expander with an expansion ratio of ex, at a distance of r_o, and a diameter of d_{bo}. They leave at a distance of r_1, and a diameter of d_{b1} where:

$$r_1 = ex \quad r_o$$

$$d_{b1} = ex \quad d_{bo}$$

If several beam expanders are used in series, the total beam expansion ratio is the product of the individual expansion ratios.

θ_1, the angle which would exist between the beams and the optical axis if lens 2 and the medium were absent is given by:

$$\theta_1 = \tan^{-1} \left(\frac{r_1}{f_1}\right)$$

The beams enter lens 2 at a distance of r_2 from the optical axis, defined by:

$$r_2 = \ell(\tan \theta_1) \ .$$

f_{eff}, the effective focal length with respect to lenses 1 and 2, and θ_2, the angle between the beams and the optical axis, are found by using the lens equation and noting the geometry:

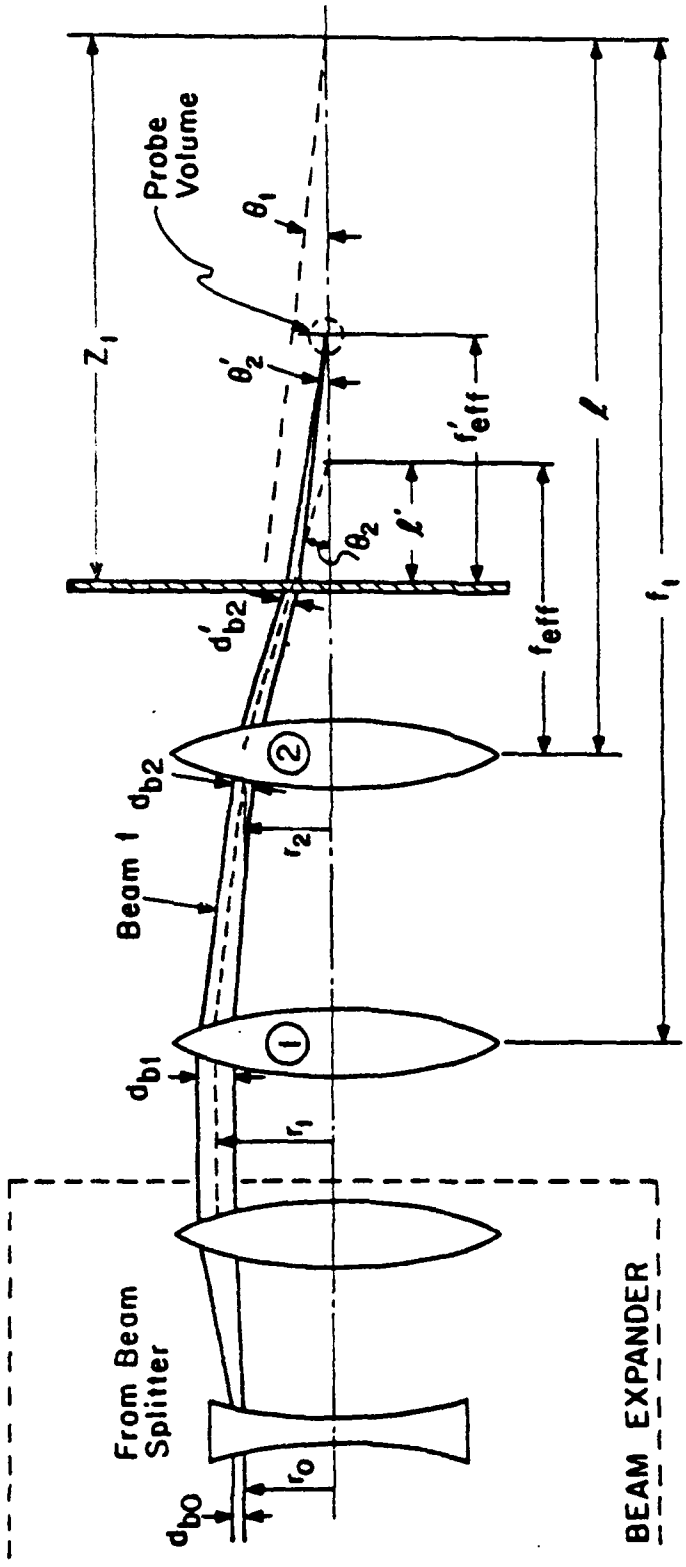

Figure 14. Schematic of Beam Paths.

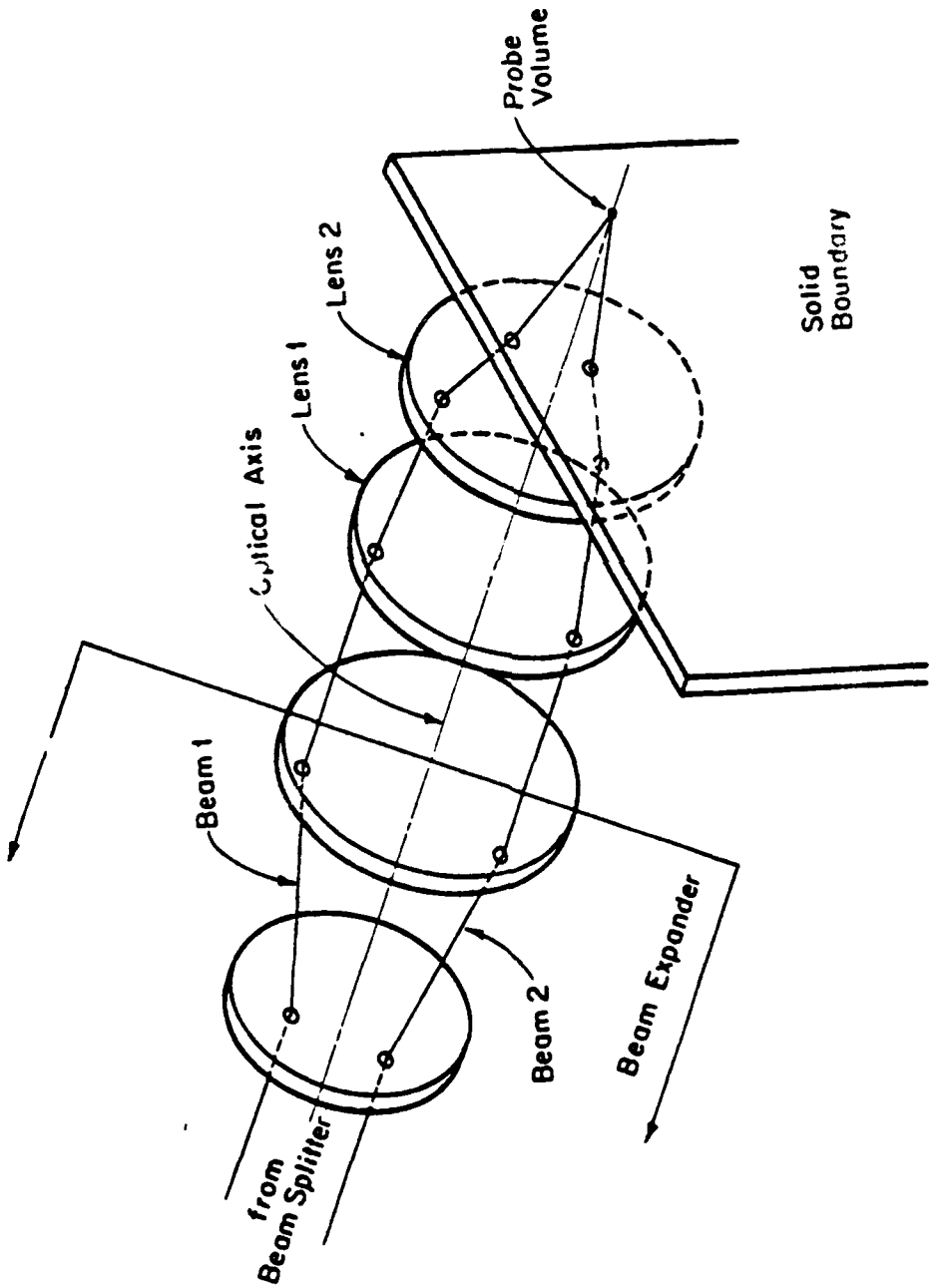

Figure 15. Isometric View of Beam Paths for Measurement of One Velocity Component.

$$f_{eff} = \frac{f_2 \cdot \ell}{(f_2 + \ell)}$$

$$\theta_2 = \tan^{-1} \left(\frac{r_2}{f_{eff}}\right)$$

Using Snell's law of refraction and assuming the index of refraction of air to equal one, the angle, θ_2', at which the beams enter the medium, and λ', the wavelength at which they propagate through the medium are calculated to be:

$$\theta_2' = \sin^{-1} \left(\frac{\sin \theta_2}{i}\right)$$

$$\lambda' = \frac{\lambda}{i}$$

ℓ', the location of the probe volume before refraction by the medium is given by:

$$\ell' = z_1 - (\ell - f_{eff})$$

This gives rise to the determination of f_{eff}', the effective focal length with respect to lens 1, lens 2, and the medium, and d_{b2}', the diameter of the beam entering the medium:

$$f_{eff}' = \frac{r_2'}{\tan \theta_2'} = \frac{\ell' \tan \theta}{\tan \theta_2'}$$

$$d_{b2}' = \frac{\ell'}{f_{eff}} d_{b2} = \frac{\ell'}{f_{eff}} \left(\frac{\ell}{f_1} d_{b1}\right)$$

From Figure 16, Δ', the angle of the "cone" formed by the focused beam, is found (assuming small Δ'):

$$\Delta' = \frac{d_{b2}' \cos \theta_2'}{f_{eff}'}$$

The expression for d_1 is given by:

$$d_1 = \frac{4}{\pi} \frac{\lambda'}{\Delta'}$$

κ_2', the half angle between beams 1 and 2, and beams 1 and 3, is found through geometry:

$$\kappa_2' = \sin^{-1} \left(\frac{\sin \theta_2'}{2}\right)$$

and the probe volume dimensions as seen in Figure 16 are:

$$d_m = \frac{d_1}{\cos \kappa_2'} \; ; \; \ell_m = \frac{d_1}{\sin \kappa_2'} \; ; \; w_m = d_1$$

The fringes within the probe volume are plane, parallel, and equidistant. The fringe spacing was calculated earlier in Equation (47) as

$$d_f = \frac{\lambda}{2 \sin \kappa_2'}$$

Hence, the number of fringes, N_f, in the probe volume can easily be calculated:

$$N_f = \frac{d_m}{d_f}$$

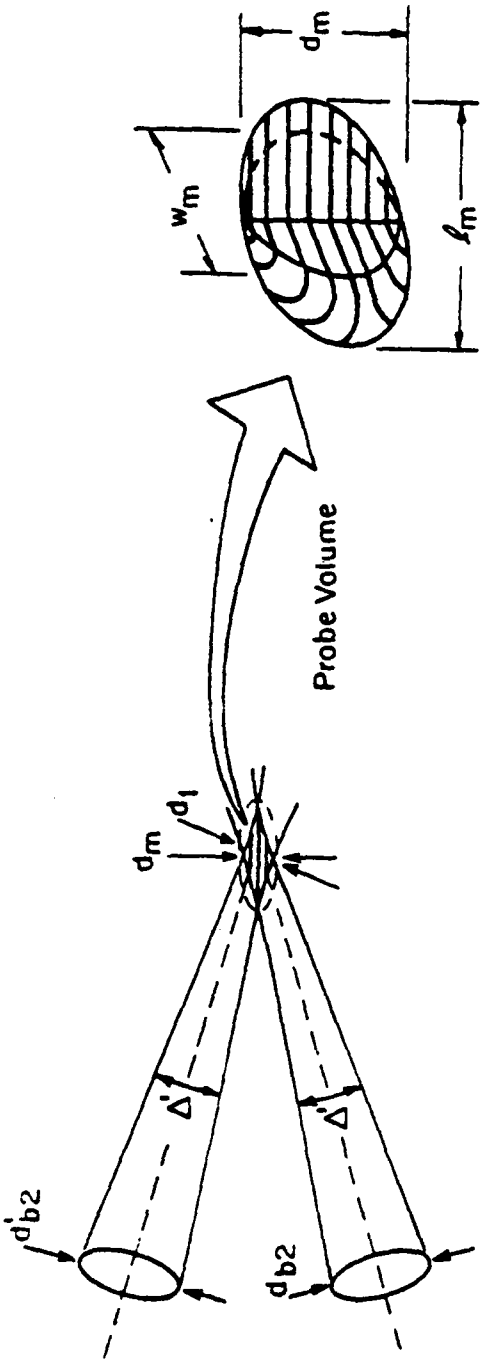

Figure 16. Intersection of Two Focused Beams and Formation of Ellipsoidal Probe Volume.

Optics

Figure 17 depicts the LDA optical train to be used to measure one velocity component. The beam from the laser is split in two and subsequently focused by a converging lens into an ellipsoidal probe volume with parallel fringe planes. The Doppler signals from particles traversing the probe volume are collected by the photomultiplier and passed to the electronic counter. The analog output from the photomultiplier is also viewed using an oscilloscope. The digital output is sent to the computer, where it is stored, via an interface designed and built in this laboratory by G. Muntz, D. Dewey, and C.F. Dewey, Jr.

All of the optical components, except for that part of the retarder attached to the laser, are physically coupled to one another creating an optical train.

The various components of the transmitter portion of the optical train shown in Figure 17 were chosen to produce a variety of probe volume dimensions and fringe spacings within the probe volumes. With two different front lenses with focal lengths, f, of 160 mm and 80 mm, and using prism spacings, V_o, (the inner prisms of the beam translator) of 6.5 mm to 19.5 mm from the optical axis, the operating conditions given in Table 2 can be achieved.

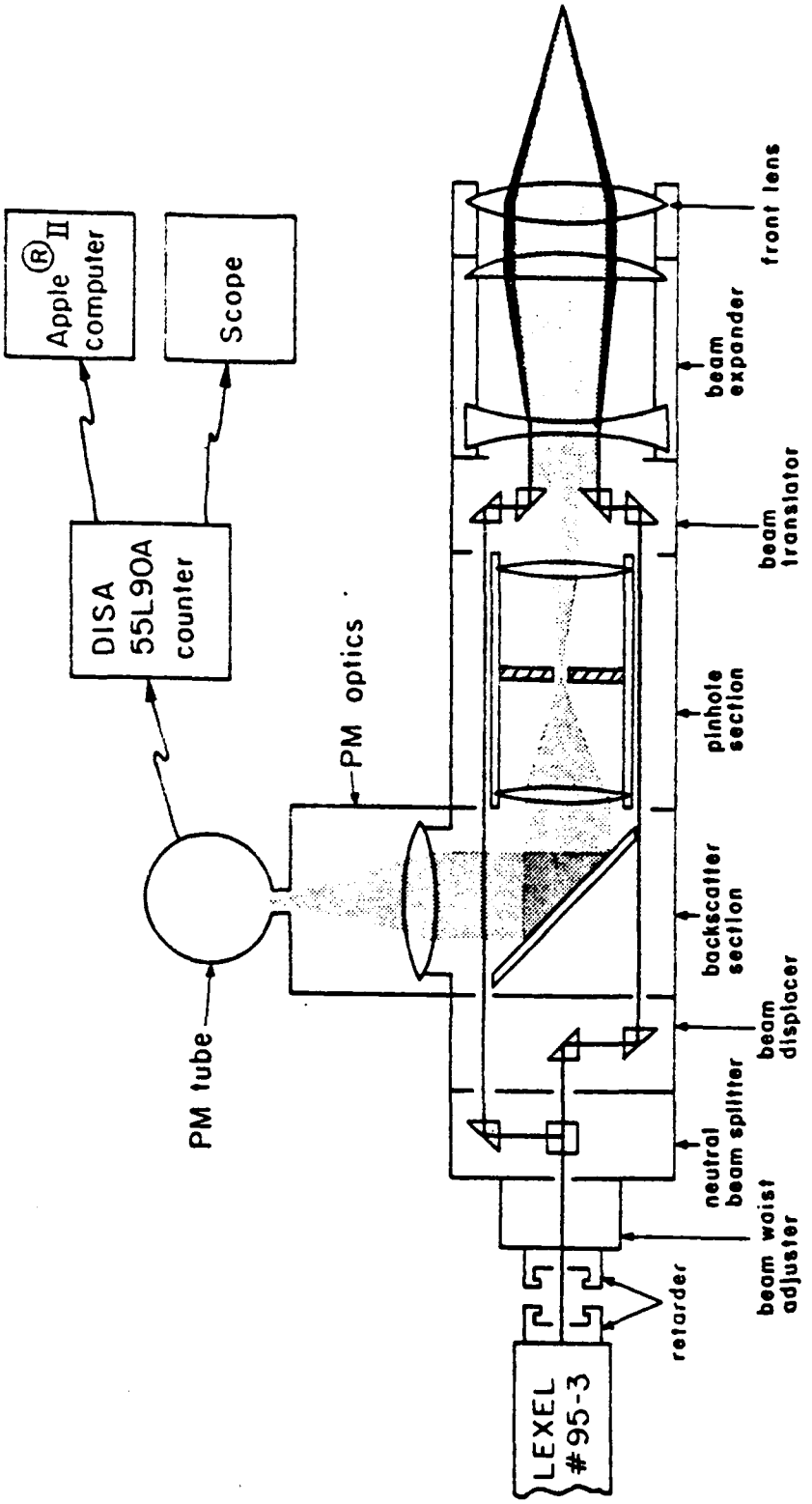

Figure 17. LDA Set-up for Backscatter Mode, One Velocity Component.

TABLE 2. PROBE VOLUME DIMENSIONS[1,3] (SIMPLE SET-UP[2])

See Fig. 16 for symbol definitions.

f (mm)	r_o (mm)	ex	ℓ_m (μm)	d_m (μm)	w_m (μm)	d_f (μm)	N_f
160	6.5	1.0	2555.74	73.39	73.36	8.96	8
160	6.5	1.9	711.01	38.75	38.69	4.73	8
160	13.0	1.0	1284.19	73.66	73.54	4.49	16
160	13.0	1.9	361.82	39.26	39.03	2.38	16
160	19.5	1.0	863.14	74.11	73.84	3.01	24
80	6.5	1.0	642.09	36.83	36.77	4.49	8
80	6.5	1.9	180.91	19.63	19.52	2.38	8
80	13.0	1.0	327.36	37.37	37.13	2.27	16
80	13.0	1.9	96.77	20.64	20.19	1.23	16
80	19.5	1.0	225.26	38.26	37.72	1.54	24

[1]Calculated for a beam diameter of 1.43 mm leaving the beam waist adjuster and a medium with index of refraction =1.

[2]A more complicated set-up will be examined in later calculations.

[3]ex is the expansion ratio of the beam diameter

In Figure 17 the transmitted beams are indicated by the dark solid lines. The paths go through a retarder, a beam waist adjuster, a neutral beamsplitter, a beam displacer, a beam translator, a beam expander, and a front lens. The retarder consists of two quarter-wave plates; the first plate circularly polarizes the incoming laser beam and the second linearly polarizes it in the correct polarization direction relative to the optical axis. The polarization rotates with the optical train due to the physical attachment between the second quarter-wave plate and the afore mentioned train.

The beam waist adjuster causes the beam waist of the two focused beams to be located at the focal point of the front lens. The neutral beamsplitter splits the incoming beam into a 50:50 intensity ratio. The beam displacer

shifts the beam lying on the optical axis a fixed radial distance away. When this is done, the radii from the optical axis to the new beam locations form right angles with each other. The beam translator allows the length of the radii to the beams to be varied and consequently affects both the diemsnions of the probe volume and the number and spacing of the fringes. The beam expander is used in cases where it is desirable to decrease the dimensions of the probe volume by increasing the intersection angle of the beams. The final component in the transmitter path, the front lens, is of prime importance since it not only focuses the beams to form a probe volume but acts as a collection agent in the receiving path. The lenses must be as free from aberrations as possible to ensure high quality signals. In addition, it is advantageous to employ achromatic lenses to correct for aberrations arising from the variation of the refractive index of glass with wavelength. This is pecially important for work with fluorescent signals where the excitation wavelength differs from the signal wavelength.

The Optical Receiver

The receiver portion of the optical train collects the backscattered (or emitted) light from the particles and hence contains the sought after velocity information. It consists of the front lens, the beam expander, the pinhole section, the backscatter section, the photomultiplier optics, and the photomultiplier tube. The receiver path is denoted in Figure 17 by the shaded area.

The front lens collects the backscattered or emitted light directly, making it necessary to have it coated with an anti-reflection film. After collection by the front lens, the light is passed through the beam expander. The beam expander section is used in conjunction with the beam translator to increase the convergence angle of the transmitted beams. It does not alter the collection efficiency or effective collection angle of the optical receiver.

The front lens of the pinhole section focuses the collection rays through a tiny pinhole removing a large fraction of the unwanted light generated through spurious reflections. The rays are sent to the backscatter

section consisting of a plane mirror angled at 45° to the optical axis. The mirror directs the light through the photomultiplier optics where they are focused through another pinhole. This pinhole acts as a spatial filter further eliminating light scattered or reflected from the various optical surfaces.

The light is finally conveyed to the photomultiplier where the incoming optical signal is converted to an electrical signal.

Versatility of Optical Components

After analyzing the performance and prices of the two major companies specializing in LDA apparatus, the optics and electronics were ordered from DISA Electronics. Careful consideration was given to both the quality of the components and the flexibility of the entire system. Since the immediate objective of the experimental work in this project was to determine whether or not the use of fluorescent particles as tracers worked in an LDA set-up, the initial system had to be kept simple. The ultimate objective, however, is to be able to measure shear stresses in two-dimensional flows, perhaps with turbulent characteristics.

In such a case it is necessary to create an orthogonal fringe system in as small a probe volume as possible, with frequency shifting of one or more beams to distinguish a positive velocity from a negative. With this in mind, the set-up depicted in Figure 18 was envisioned. In this set-up, a neutral beamsplitter is first employed to split the laser beam (cyan-colored if a two-color set-up is desired) into equal intensity ratios. In the mono-color set-up, another neutral beamsplitter follows the first; in the two-color set-up, the neutral beamsplitter is followed by a dichroic beamsplitter. The second beamsplitter divides only one of the beams, either into equal intensity ratios in the mono-color case or into a green beam and a blue beam in the two-color case.

With the two-color set-up, the cyan and the blue beams intersect to form a series of parallel fringe planes orthogonal to the fringe planes formed by the cyan and the green beams. Similarly, in the mono-color set-up, the most intense beam combines with each of the two beams to form two orthogonal sets of fringe planes. A two-color backscatter system can distinguish between scattering from the two orthogonal fringe sets on the basis of wave-

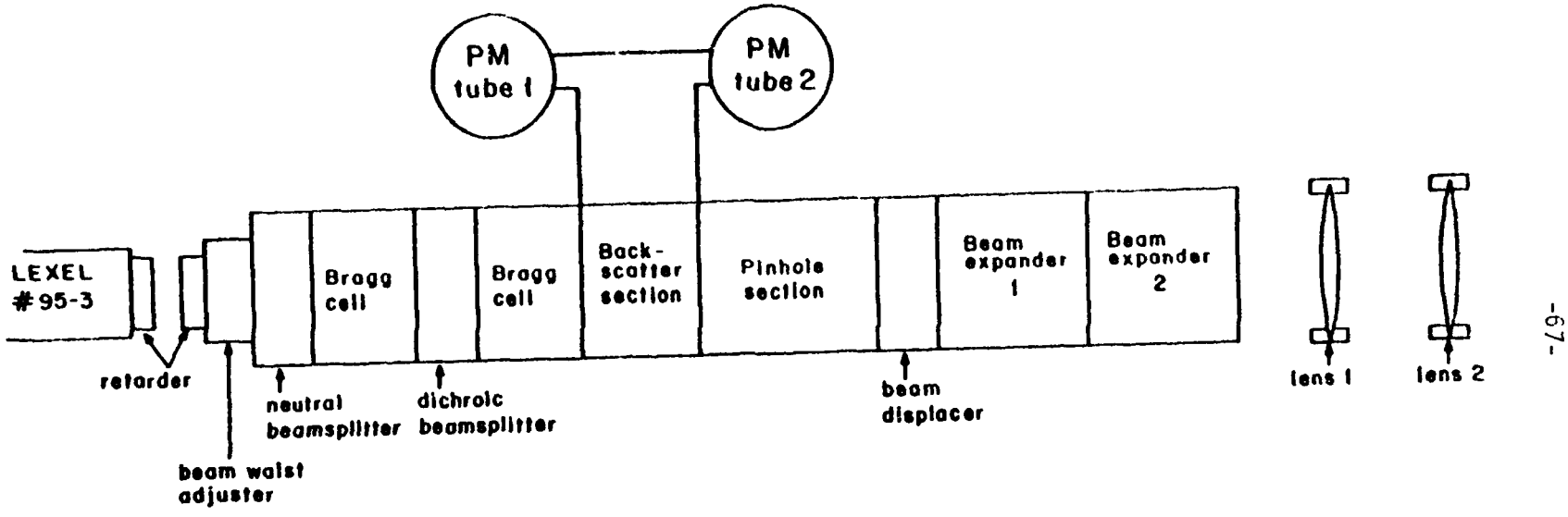

Figure 18. LDA Optical Set-up for Measurement of Two Velocity Components with Frequency-Shifting, Backscatter Mode.

length. With the mono-color system (i.e., a single wavelength), Bragg cells must be used to shift the apparent laser frequency to obtain discrimination between the two velocity dimensions.

Bragg cells are usually employed to optically shift one beam at a time by 40 MHz. This produces a set or sets of moving fringe planes. A stationary particle situated in the probe volume produces a frequency equal to the shift frequency. Movement in the same direction as the fringes lowers the signal frequency and in the opposite direction raises it. Both particle speed and direction can subsequently be deduced.

Two beam expanders in combination with lenses of high f-number (focal length/diameter) significantly reduce the dimensions of the probe volume. Table 3 displays the dimensions of the probe volume as well as the number and spacing of the fringes following the calculations described previously.

TABLE 3. PROBE VOLUME DIMENSIONS[1] (COMPLICATED SET-UP[2])

See Fig 16.

r_o (mm)	ex	z_m (μm)	d_m (μm)	w_m (μm)	d_f (μm)	N_f
6.5	1.0	548.47	29.51	29.46	3.60	8
6.5	1.9	156.07	15.80	15.72	1.92	8
6.5	1.9[2]	47.27	15.99	8.65	1.06	15
13.0	1.0	282.63	30.08	29.91	1.83	16
13.0	1.9	86.44	16.86	16.55	1.01	16
19.5	1.0	197.76	31.02	30.64	1.25	24

[1]Calculated for a beam diameter of 1.43 mm leaving the beam waist adjuster and a medium with index of refraction = 1.33.

[2]Front lenses with f_1 = 160 mm, f_2 = 80 mm; Distance, ℓ = 120 mm; Distance, z_1, = 95 mm (see Figure 14).

Geometrical Configuration

Figure 19 is a schematic of the geometrical configuration of the laser and optics. Both laser and optics had to be securely fastened to a vibration-free base since the smallest movement resulted in misalignment and a distortion in or even loss of the fringe pattern in the probe volume. They were bolted to a 2-1/2' x 4' granite table sitting on shock-absorbent pads. The pads, purchased from Air-Loc®, were designed to withstand loads up to 1500 lbs and absorb 85% of the vibration.

The mirrors were purchased from Newport Research Corporation and were rated 99% reflective at visible wavelengths. The optical train rested on an optical rail to permit ease in translation of the components.

C. Continuing Research

Fabrication of the optical stands and integration of the optical system are the next objectives. Following this, measurements will be made with targets of known velocity to calibrate the LDA system. Then measurements will be made using fluorescent particles and an estimate of signal-to-noise ratio will be made. Finally, the LDA will be applied to practical shear flows near solid boundaris where, heretofore, LDA has not been a practical method of measurement.

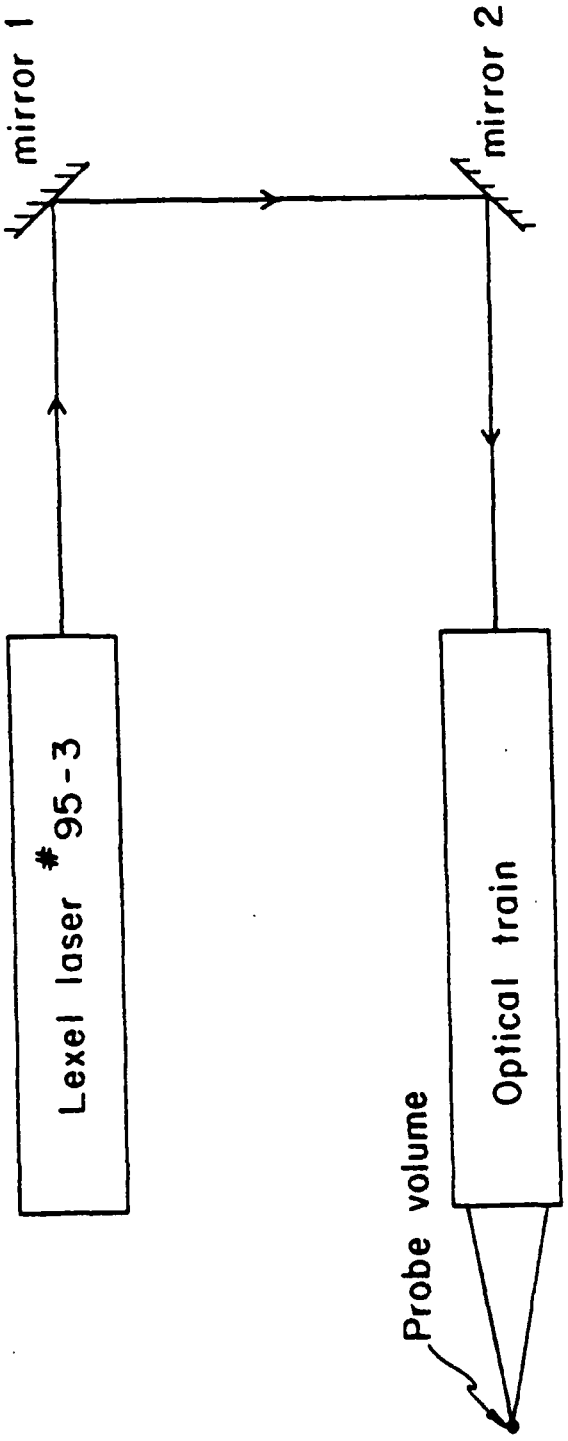

Figure 19. Geometrical Configuration of LDA Set-up.

IV. SUMMARY

Fluid shear stress is one of the most important quantities characterizing the interaction between a flowing fluid and a solid body. A knowledge of surface shear stress is essential in determining the drag on submerged bodies, the energy losses in internal flows, local surface heat transfer rates in both internal and external flows, flow separation, cavitation, and unsteady flow behavior in rotating machinery.

In spite of many previous investigations of both laser Doppler anemometry (LDA) and surface hot-film gauges, the use of these methods for determining wall shear stress is poorly developed. Conventional LDA measurements near surfaces are plagued by spurious background scattering and marginal resolution. Use of surface hot-film gauges is severely inhibited by the necessity of empirical calibration and an incomplete understanding of their response in turbulent and unsteady flows.

This research program will develop new methodology for the use of these two complementary techniques as quantitative measurement tools for determining local surface shear stress. The LDA system will be based on detecting laser-induced fluorescence from solid particles in a so-called "backscatter" mode. Two individual velocity components will be measured by using multiplexing in the frequency domain. The hot-film probes will employ multiple elements such that conventional calibration procedures can be eliminated. Both theory and experiment are being used to determine the utility of LDA and hot-film instrumentation in unsteady flows.

Our analysis of hot-film probe performance considers an arbitrarily shaped probe (or set of probes) flush-mounted on a plane thermally conducting substrate, possessing an arbitrary heat flux distribution, and exposed to a steady uniform fluid shear. We have formulated the complete, three-dimensional fluid and substrate energy equations and have coupled them through their associated boundary conditions. A novel solution procedure that combines Fourier transformation of the governing equations, their analytical solution in transform space, and, finally, numerical inversion to predict physical space temperature distributions and heat fluxes is being

developed. This approach has some clear potential advantages -- as well as some possbile weaknesses -- that are being systematically explored. One important advantage is that the solutions obtained can be limited to any plane of interest (particularly the fluid-solid interface); solutions for temperature and heat flux distributions elsewhere in the fluid or substrate need not be generated unless desired. This method should thus prove to be computationally efficient for determining what is of greatest interest in probe analysis - the probe temperature and heat flux distributions. Since the full three-dimensional fluid and solid energy equations are considered, the technique should be able to handle a wide range of fluids and flow speeds, probe geometries and substrate properties. The use of this technique will enable us to obtain detailed descriptions of the temperature fields and heat flows associated with a given probe design. It will also enable us to investigate the sensitivity of probe performance to various flow and substrate parameters and to thus determine a set of "optimum" designs which could then be "numerically calibrated". Potential weaknesses of this appraoch approach may be associated with numerical difficulties in obtaining highly accurate, yet efficient, solutions to the resulting two-dimensional Fourier inversion integrals for desired probe configurations.

Our laser Doppler anemometry (LDA) efforts are keyed to the use of fluorescent tracer particles in combination with optical filters to overcome the severe limitations of conventional LDA techniques near solid surfaces. Here, background scattering is large and LDA becomes very difficult because the "shot noise" (statistical uncertainty) from the background swamps the signal arising from tracer particles moving through the measurement volume.

The fluorescent emission is at longer wavelengths than the incident absorbed wavelength; consequently, optical filters can be employed to filter out the background scattering while passing the fluorescent signals. The theoretical estimates we have made predict large (factor of 1000) increases in the signal-to-noise ratio using the fluorescent tracer particles over that using conventional scattering particles.

These methods may be used with conventional backscatter optics and either one or two component systems; however, multiplexing in the Bragg shift frequency domain rather than in the optical (wavelength) domain is required because the fluorescence is at a wavelength longer than the excitation wavelength.

BIBLIOGRAPHY

Ackerberg, R.C., Patel, R.D., and Gupta, [illegible]. (1978), J. Fluid Mech., 86, 49.

Aggarwal, J.K. (1978), J. Phys. E.: Sci. Inst., 11, 349.

Agrawal, Y., Talbot, L., and Gong, K. (1978), J. Fluid Mech., 85, 497.

Armistead, R.A., Jr., and Keyes, J.J., Jr. (1968a), Rev. Sci. Inst., 39, 61.

Armistead, R.A., Jr., and Keyes, J.J., Jr. (1968b), Trans. ASME (J. Heat. Trans.), 90, 13.

Bakewell, H.P., Jr., and Lumley, J.L. (1967), Phys. Fluids, 10, 1880.

Bellhouse, B.J., and Schultz, D.L. (1966), J. Fluid Mech., 24, 379.

Bellhouse, B.J., and Schultz, D.L. (1967), J. Fluid Mech., 29, 289.

Bellhouse, B.J., and Schultz, D.L. (1968), J. Fluid Mech., 32, 675.

Berlman, I.B., Handbook of Fluorescence Spectra of Aromatic Molecules, Academic Press, 1971.

Berman, N.S., and Dunning, J.W. (1973), J. Fluid Mech., 61, 289.

Blake, W.K. (1970), J. Fluid Mech., 44, 637.

Born, G.V.R., Melling, A., and Whitelaw, J.H. (1978), Biorheology, 15, 163.

Born, M., and Wolf, E., Principles of Optics, 6th edition, Pergamon Press, 1980.

Bossel, H.H., Hiller, W.J., and Meier, G.E.A. (1972), J. Phys. E.: Sci. Inst., 5, 893.

Brech, R., and Bellhouse, B.J. (1973), Cardiovasc. Res., 7, 593.

Brown, G.L. (1967), Proc. 1967 Heat Transfer and Fluid Mechanics Institute, Stanford U. Press, p.361.

Buchave, P., George, W.K., Jr., and Lumley, J.L. (1979), "The measurement of turbulence with the laser-Doppler anemometer," in Ann. Rev. Fluid Mech., Vol 11, Ann. Reviews, Inc., Palo Alto, pp. 443-503.

Burton, T.E. (1974), "The connection between intermittent turbulent activity near the wall of a turbulent boundary layer with pressure fluctuations at the wall," Naval Ship Systems Command, Report No. 70208-10.

Carslaw, H.S., and Jaeger, J.C. (1947), Conduction of Heat in Solids, Oxford U Press, Oxord.

Clark, C. (1974), J. Phys. E.: Sci. Inst., 7, 548.

Crossway, F.L., Horukohl, J.O., and Lennert, A.E., (1972), "Signal characteristics and signal-conditioning electronics for a vector velocity laser anemometer," Proc. 1st. Int. Workshop on Laser Velocimetry, Purdue, p. 396.

Davies, P.A.O.L., and Kimber G.R. (1972), in Conference on Fluid Dynamic Meas. in the Industrial and Medical Environments, Vol I., (D.J. Cockrell, Ed.), Leicester U. Press, Leicester, p.236.

Drain, L.E. (1980), The Laser-Doppler Technique, John Wiley and Sons.

Durao, D.F.G., and Whitelaw, J.H., (1979), J. of Phys., E: Sci. Inst., 12, 47-50.

Durrani, R.S., and Greated, C.A. (1977), Laser Systems in Flow Measurement, Plenum Press, N.Y.

Durst, F., Melling, A., and Whitelaw, J.H. (1976), Principles and Practice of Laser-Doppler Anemometry, Academic Press, N.Y.

Durst, R., and Stevenson, W.H. (1979), Applied Optics, 13, No.4, pp. 516-24.

Eckelmann, H. (1974), J. Fluid Mech., 65, 439.

Eckelmann, H., and Reichardt, H. (1971), in Proc. Symp. on Turbulence in Liquids (J.L. Zukin and G.K. Patterson, Eds.), U. Missouri, Rolla, October 4-6, pp. 144-148.

Edwards, R.V., Angus, J.C., French, M.J., and Dunning, J.W., Jr. (1971), J. Appl. Phys., 42, 837.

Fagella-Alabastro, E.B., and Hellums, J.D. (1969), AIChE Journal, 15, 164.

Fortuna, G. (1970), "Effect of drag reducing polymers in flow near a wall," Ph.D. Thesis, U. Illinois, Urbana.

Fortuna G., and Hanratty, T.J. (1971), Int. J. Heat & Mass Transfer, 14, 1499.

George, W.K., Jr. (1972), in Conf. on Fluid Dyn. Meas in the Industrial and Medical Environments, Vol. I (D.J. Cockrell, Ed.), Leicester U. Press, Leicester, pp. 88-99.

George, W.K., Jr., and Lumley, J.L. (1973), J. Fluid Mech., 60, 321.

Geremia, J.O. (1970), "An experimental investigation of turbulence effects at the solid boundary using flush mounted hot film sensors," Ph.D Thesis, George Washington University.

Hanratty, T.J., and Campbell, J.A. (1982), "Measurement of wall shear stress," in Fluid. Mech. Meas. (R.J. Goldstein, Ed.), Hemisphere Publ. Corp. (in press).

Hendricks, C.D., and Babil, S. (1972), J. Phys. E.: Sci. Inst., 5, 905.

Humphrey, R.L. (1978), "Thermal and Optical Anemometry Techniques," First Mid-Atlantic Conference on Bio-Fluid Mechanics, Virginia Polytechnic Institute.

Johnson, D.A. (1973), AIAA Journal, 11, 890.

Johnson, D.A., and Rose, W.C. (1975), AIAA Journal, 13, 512.

Karpuk, M.E., and Tiederman, W.G., Jr. (1976), AIAA Journal, 14, 1099.

Kline, S.J., Reynolds, W.C., Schraub, F.A., and Runstadler, P.W. (1967), J. Fluid Mech., 30, 741.

Kreid, D.K. (1974), Appl. Optics, 13, 1872.

Leehey, P. (1966), "A review of flow noise research related to the sonar self noise problem," Dept. Navy, Bureau of Ships, Publ. NObsr-93055.

Leveque, M.A. (1928), Annales des Mines, 13, 201.

Liepmann, H.W., and Skinner, G. (1954), "Shearing stress measurements by use of heated element," NACA TN 3268.

Lighthill, M.J. (1954), Proc. Roy. Soc. A., 224, 1.

Ling, S.C. (1955), "Measurement of flow characteristics by the hot-film technique," Ph.D. Thesis, Iowa State University.

Ling, S.C. (1963), J. Heat Trans., 85C, 230.

Ling, S.C., Atabeck, H.B., and Carmody, J.J. (1969), Proc. XII Int. Cong. Appl. Mech. (M. Hetenyi and W.G. Vincenti, Eds.), Springer-Verlag, Berlin, pp. 277-291.

Ling, S.C., Atabeck, H.B., Fry, D.A., Patel, D.J., and Janicki, J. (1968), Circ. Res., 23, 789.

Ludweig, H. (1950), "Instrument for measuring the wall shearing stress of turbulent boundary layers," NACA TM-1284.

McCroskey, W.J., and Durbin, E.J. (1972), Trans. ASME (J. Basic Eng'g.), 94, 46.

Mitchell, J. E. (1965), "Investigation of wall turbulence using a diffusion controlled electrode," Ph.D. Thesis, U. Illinois.

Mitchell, J. E., and Hanratty, T. J. (1966), J. Fluid Mech., 26, 199.

Murthy, V. S., and Rose, W. C. (1977), AIAA Paper 77-691.

Murthy, V. S., and Rose, W. C. (1978), NASA TM 78,454.

Murthy, S. N. B. (1976), A Project SQUID Workshop on Turbulence in Internal Flows (S. N. B. Murthy, Ed.), Hemisphere Publ. Co., Washington.

Newman, J. (1973), in Electroanalytical Chemistry, Vol. 6, (Allen J. Bard, Ed.), Marcel Dekker, N. Y., p. 187.

Oldengarm, J., van Krieken, A. H., and van der Klooster, H. W. (1975), J. Phys. E.: Sci. Inst., 8, 203.

Owen, F. K., and Bellhouse, B. J. (1970), AIAA Journal, 8, 1358.

Phillips, J. H., and Ackerberg, R. C. (1973), J. Fluid Mech., 58, 561.

Pope, R. J. (1971), "The use of thin-film heated elements in water flows," Ph.D. Thesis, Oxford U. See also AIAA J., 10, 729 (1972).

Popovich, A. T. (1969), Ind. Eng'g. Chem. Fund., 8, 609.

Popovich, A. T., and Hummel, R. L. (1967a), Chem. Eng'g. Science, 22, 21.

Popovich, A. T., and Hummel, R. L. (1967b), AIChE J., 13, 854.

Quigley, M. S., and Tiederman, W. G., Jr. (1977), AIAA Journal, 15, 266.

Reich, S. (1979), Appl. Phys. Lett., 33, 988.

Reiss, L. P. (1962), "Investigation of turbulence near a pipe wall using a diffusion controlled electrolytic reaction on a circular electrode," Ph.D. Thesis, U. Illinois.

Reiss, L. P., and Hanratty, T. J. (1962), AIChE J., 8, 245.

Reiss, L. P., and Hanratty, T. J. (1963), AIChE J., 9, 154.

Rose, W. C., and McDaid, E. P. (1977), AIAA Journal, 15, 1368.

Sdougos, H. P. (1977), "Secondary flow and turbulence in a cone-and-plate Couette flow device," M.S. Thesis, MIT.

Seed, W. A., and Wood, N. B. (1970), J. Phys. E.: Sci. Inst., 3, 377.

Sirkar, K. K., and Hanratty, T. J. (1970a), J. Fluid Mech., 44, 589.

Sirkar, K. K., and Hanratty, T. J. (1970b), J. Fluid Mech., 44, 605.

Skinner, G. T., "A new method of calibrating thin film gauge backing materials," Cornell Aero. Lab. Rept. CAL-105, June, 1962. See also: ARS J., 31, 671 (1961).

Smart, A. E. (1978), "Laser anemometry close to walls," Dynamic Flow Conference, Baltimore, September, 1978 (to be published).

Smith, K.A., Colton, C. K., and Friedman, R. W. (1974), "Shear stress measurements at bifurcations," paper presented at Specialists Meeting: Fluid Dynamic Aspects of Arterial Disease, Ohio State U., Columbus.

Spence, D.A., and Brown, G.L. (1968), J. Fluid Mech., 33, 753.

Springer, S.G. (1974), Proc. Roy. Soc. Lon, A, 337, 395.

Stevenson, W.H., deSantos, R., and Mettler, S.C. (1975), Appl. Phys. Lett., 27, 395. See also by the same authors "Fringe mode fluorescence velocimetry", Proc. NATO/AGARD Symposium on Applications of Non-Intrusive Instrumentation on Fluid Flow, St. Louis, France, AGARD Conf. Proc. No. 193, 1976.

Stuart, J.T. (1955), Proc. Roy. Soc. A, 231, 116.

Tanner, R.I. (1967), Trans. ASME (J. Appl. Mech.), 34, 801.

Tribus, M., and Klein, J. (1953), Heat Transfer - A Symposium: Summer, 1952, Engineering Research Institute, Univ. Michigan, Ann Arbor, pp. 211-235.

Woodrofe, G. (1970), "Some problems in pulsatile flow," Ph.D. Thesis, Oxford U.

Yoganathan, A.P., Corcoran, W.H., and Harrison, E.C. (1979), J. Biomechanics, 12, 135.

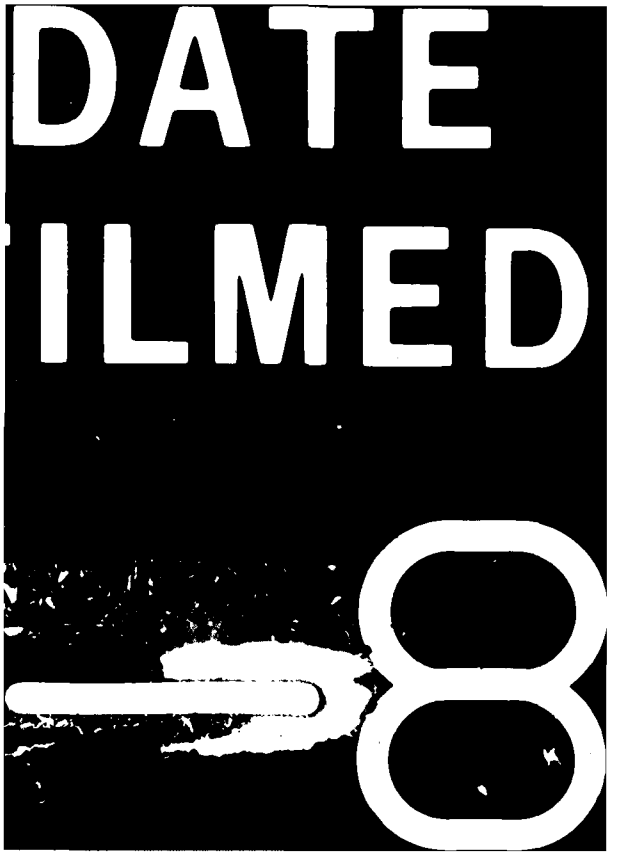
DATE
ILMED
8